Commun. Comput. Phys.
doi: 10.4208/cicp.170610.021210a

Vol. **10**, No. 3, pp. 635-671
September 2011

On Universal Osher-Type Schemes for General Nonlinear Hyperbolic Conservation Laws

Michael Dumbser* and Eleuterio F. Toro

Laboratory of Applied Mathematics, University of Trento, I-38100 Trento, Italy.

Received 17 June 2010; Accepted (in revised version) 2 December 2010

Available online 1 June 2011

Abstract. This paper is concerned with a new version of the Osher-Solomon Riemann solver and is based on a numerical integration of the path-dependent dissipation matrix. The resulting scheme is much simpler than the original one and is applicable to *general* hyperbolic conservation laws, while retaining the attractive features of the original solver: the method is entropy-satisfying, differentiable and complete in the sense that it attributes a different numerical viscosity to each characteristic field, in particular to the intermediate ones, since the full eigenstructure of the underlying hyperbolic system is used. To illustrate the potential of the proposed scheme we show applications to the following hyperbolic conservation laws: Euler equations of compressible gas-dynamics with ideal gas and real gas equation of state, classical and relativistic MHD equations as well as the equations of nonlinear elasticity. To the knowledge of the authors, apart from the Euler equations with ideal gas, an Osher-type scheme has never been devised before for any of these complicated PDE systems. Since our new general Riemann solver can be directly used as a building block of high order finite volume and discontinuous Galerkin schemes we also show the extension to higher order of accuracy and multiple space dimensions in the new framework of $P_N P_M$ schemes on unstructured meshes recently proposed in [9].

AMS subject classifications: 35L65, 65M08, 76M12, 76L05

Key words: Universal Osher-Solomon flux, universal Roe flux, high resolution shock-capturing finite volume schemes, WENO schemes, reconstructed discontinuous Galerkin methods, $P_N P_M$ schemes, Euler equations, gas dynamics, ideal gas and real gas equation of state, MHD equations, relativistic MHD equations, nonlinear elasticity.

1 Introduction

Finite volume and discontinuous Galerkin methods for hyperbolic conservation laws require a numerical flux. There are essentially two approaches to obtain the flux, the centered or symmetric approach and the upwind or Godunov approach. Schemes derived

*Corresponding author. *Email addresses:* michael.dumbser@ing.unitn.it (M. Dumbser), toroe@ing.unitn.it (E. F. Toro)

from the centered approach do not explicitly use wave propagation information and are much simpler and general than schemes derived from the upwind approach. Among the centered schemes we have for example the original Lax-Friedrichs scheme [29] as well as the FORCE scheme of Billet and Toro [44] and its multi-dimensional extensions [3,12,45]. An exhaustive overview of existing Riemann solvers can be found in [43], for example. The upwind methods use explicitly wave propagation information via the solution of the local Riemann problem, solved exactly or approximately, resulting in more complex schemes and restricted to systems for which the Riemann problem can be solved. However, upwind schemes are more accurate than centered schemes and are to be preferred when the appropriate upwind information is available. This is patently evident when attempting to capture waves associated with linearly degenerated fields, such as slip surfaces and material interfaces. This is much more challenging than resolving non-linear waves such as shock waves. The numerical diffusion of centered schemes, even if high-order extensions are used, can become unacceptable as time evolves. However it is important to clarify that not all upwind methods will resolve waves associated with linearly degenerated fields equally well. It rather depends on the particular Riemann solver used. This calls for a distinction between *complete* Riemann solvers and *incomplete* Riemann solvers. Solvers in the first class have an underlying wave model that contains all the characteristic fields of the exact Riemann solver of Godunov [20]. Incomplete solvers adopt reduced wave models and are usually based on the largest signal speeds present in the system. Classical examples of incomplete Riemann solvers are the Rusanov scheme [37], which has a one-wave model, and the HLL solver [25], which has a two-wave model, and its extensions [17,46]. Another useful distinction is a linear solver and a nonlinear solver. Linearized solvers [35] require explicit entropy fixes and fail for low density flows. Thus the ideal Riemann solver is non-linear and complete.

The Osher-Solomon scheme [31] is a non-linear and complete Riemann solver. Additional attractive features of the scheme are robustness, entropy satisfaction, good behavior for slowly-moving shocks and smoothness (differentiability with respect to its arguments); properties that make it very attractive to the aeronautical community. The Osher-Solomon method begins from the assumption that the flux can be split into a positive part and a negative part, and that both components are associated with corresponding Jacobian matrices with positive or zero eigenvalues and negative or zero eigenvalues, respectively. The proposed numerical flux then involves computing path dependent integrals in phase-space. In order to evaluate the integrals analytically Osher and Solomon consider a path that is a union of disjoint local paths k, assumed to be tangential to a corresponding eigenvector. Then the approach also requires intermediate states $k-1$ and k which are joined by the partial path k. Moreover, for a genuinely non-linear field one generally requires, in addition, a local sonic state. To find the correct intermediate states and potential sonic states one would effectively have to solve the Riemann problem analytically with an exact Riemann solver, which would make the approach unfeasible in practice, since with the exact Riemann solver at hand, one could directly apply the Godunov flux [20]. For this purpose Osher and Solomon assume a reduced solver composed

of simple waves for which Riemann invariants are applicable. Thus, for a system of m equations one needs to compute $m-1$ intermediate states and one sonic state for each genuinely non-linear field. Then, exact integration is performed for each characteristic field using the partial paths. For the Euler equations for ideal gases one ends up with 16 cases. As indicated earlier, the Osher-Solomon scheme has several very attractive features. However, the solver is indeed very complex and computationally expensive. Probably for this reason it has remained rather unattractive to the numerical community, and particularly to the engineering and scientific community interested in applications involving very complex hyperbolic systems.

In this paper we present a new version of the Osher-Solomon Riemann solver. The new scheme is based on the numerical integration of a path-dependent dissipation matrix. The resulting scheme is much simpler than the original one and is applicable in a straightforward manner to any hyperbolic system for which the eigenstructure is analytically available. However, our approach is also applicable to systems for which the eigenstructure is not available analytically since in this case the eigenstructure is simply computed numerically using standard linear algebra packages, such as the subroutine **RG** from the EISPACK package. In this way the new Osher-Solomon solver can thus also be implemented for very complex hyperbolic PDE. The proposed scheme retains all the attractive features of the original solver; it is non-linear, complete, entropy satisfying, differentiable with respect to its arguments and very robust. To illustrate the potential of the proposed scheme we show applications to the Euler equations for ideal and real gases, the classical and relativistic MHD equations as well as the equations of non-linear elasticity. We also report the extension of the scheme to high order of accuracy in space and time on general unstructured meshes in multiple space dimensions.

The outline of this paper is as follows: in Section 2 we briefly review the original Osher-Solomon scheme. In Section 3 we present a new generalized version of the Osher-Solomon solver for one-dimensional hyperbolic systems. The proposed approach to generalized the Osher-Solomon scheme naturally leads to an analogous formulation for the Riemann solver of Roe [35] in its weak form, as first introduced by Toumi in [48]. In Section 4 we show first order results of our schemes for a large set of complicated hyperbolic systems and in Section 5 we then present the extension to multiple space dimensions and higher order of accuracy. Conclusions are drawn in Section 6.

2 Brief review of Osher's solver

In this section we briefly review the Osher-Solomon Riemann solver and introduce appropriate notation.

2.1 Notation and basic definitions

Consider a general $m \times m$ hyperbolic system of conservation laws

$$\partial_t \mathbf{Q} + \partial_x \mathbf{F}(\mathbf{Q}) = \mathbf{0}, \tag{2.1}$$

with the vectors of conserved variables and fluxes respectively denoted as

$$\mathbf{Q}=[q_1,q_2,\cdots,q_m]^T\in\Omega_q,\qquad \mathbf{F}(\mathbf{Q})=[f_1,f_2,\cdots,f_m]^T. \tag{2.2}$$

Here, Ω_q is the so-called domain of definition of PDE (2.1) and is supposed to be a convex set. The system is supposed to be hyperbolic for all $\mathbf{Q}\in\Omega_q$. The real eigenvalues, written in increasing order, are denoted by $\lambda_i(\mathbf{Q})$ and the corresponding right eigenvectors by $\mathbf{R}_i(\mathbf{Q})$, for $i=1,2,\cdots,m$. Hyperbolicity of system (2.1) is equivalent to saying that the Jacobian matrix $\mathbf{A}(\mathbf{Q})$ of the flux $\mathbf{F}(\mathbf{Q})$ is diagonalizable, that is

$$\mathbf{A}(\mathbf{Q})=\mathbf{R}(\mathbf{Q})\mathbf{\Lambda}(\mathbf{Q})\mathbf{R}^{-1}(\mathbf{Q}), \tag{2.3}$$

where $\mathbf{R}(\mathbf{Q})$ is the matrix formed by the right eigenvectors, $\mathbf{R}^{-1}(\mathbf{Q})$ is its inverse and $\mathbf{\Lambda}(\mathbf{Q})$ is the diagonal matrix whose diagonal entries are the eigenvalues λ_i.

We now introduce the definitions

$$\lambda_i^+(\mathbf{Q})=\max\{\lambda_i(\mathbf{Q}),0\},\qquad \lambda_i^-(\mathbf{Q})=\min\{\lambda_i(\mathbf{Q}),0\} \tag{2.4}$$

and the associated diagonal matrices $\mathbf{\Lambda}^+(\mathbf{Q})$, $\mathbf{\Lambda}^-(\mathbf{Q})$ and $|\mathbf{\Lambda}(\mathbf{Q})|$, whose diagonal entries are $\lambda_i^+(\mathbf{Q})$, $\lambda_i^-(\mathbf{Q})$ and $|\lambda_i(\mathbf{Q})|$ respectively. Note that

$$|\lambda_i(\mathbf{Q})|=\lambda_i^+(\mathbf{Q})-\lambda_i^-(\mathbf{Q}) \tag{2.5}$$

and hence

$$|\mathbf{\Lambda}(\mathbf{Q})|=\mathbf{\Lambda}^+(\mathbf{Q})-\mathbf{\Lambda}^-(\mathbf{Q}). \tag{2.6}$$

It is also convenient to introduce

$$|\mathbf{A}(\mathbf{Q})|=\mathbf{R}(\mathbf{Q})|\mathbf{\Lambda}(\mathbf{Q})|\mathbf{R}^{-1}(\mathbf{Q}). \tag{2.7}$$

Then the diagonalization process is extended as

$$\mathbf{A}^+(\mathbf{Q})=\mathbf{R}(\mathbf{Q})\mathbf{\Lambda}^+(\mathbf{Q})\mathbf{R}^{-1}(\mathbf{Q}),\qquad \mathbf{A}^-(\mathbf{Q})=\mathbf{R}(\mathbf{Q})\mathbf{\Lambda}^-(\mathbf{Q})\mathbf{R}^{-1}(\mathbf{Q}). \tag{2.8}$$

It follows that

$$\mathbf{A}(\mathbf{Q})=\mathbf{A}^+(\mathbf{Q})+\mathbf{A}^-(\mathbf{Q}), \tag{2.9}$$

where $\mathbf{A}^+(\mathbf{Q})$ has positive or zero eigenvalues and $\mathbf{A}^-(\mathbf{Q})$ has negative or zero eigenvalues. This is a direct generalization to non-linear systems of the Jacobian splitting for linear systems with constant coefficients. Note that we can also write

$$|\mathbf{A}(\mathbf{Q})|=\mathbf{A}^+(\mathbf{Q})-\mathbf{A}^-(\mathbf{Q}). \tag{2.10}$$

The computational domain Ω is now discretized with equidistant elements $T_i=[x_{i-1/2};x_{i+1/2}]$ of mesh size $\Delta x=x_{i+1/2}-x_{i-1/2}$ and the time step is denoted by $\Delta t=$

$t^{n+1}-t^n$. Then a finite volume scheme can be obtained for (2.1) by integration over the space-time control volume $[x_{i-1/2};x_{i+1/2}]\times[t^n;t^{n+1}]$ as

$$\mathbf{Q}_i^{n+1}=\mathbf{Q}_i^n-\frac{\Delta t}{\Delta x}\left(\mathbf{F}_{i+\frac{1}{2}}-\mathbf{F}_{i-\frac{1}{2}}\right), \tag{2.11}$$

where $\mathbf{F}_{i+1/2}$ is the numerical flux. Upwind methods define a numerical flux by solving the local Riemann problem for (2.1) with initial condition

$$\mathbf{Q}(x,0)=\begin{cases}\mathbf{Q}_0, & \text{if } x\leq 0,\\ \mathbf{Q}_1, & \text{if } x>0.\end{cases} \tag{2.12}$$

At present there are several ways of solving (2.1), (2.12) and computing $\mathbf{F}_{i+1/2}$. For background see [43] and references therein, for example.

2.2 The classical Osher-Solomon solver

The Osher-Solomon numerical flux [31] is obtained by first assuming the flux splitting

$$\mathbf{F}(\mathbf{Q})=\mathbf{F}^+(\mathbf{Q})+\mathbf{F}^-(\mathbf{Q}), \tag{2.13}$$

with corresponding Jacobians

$$\mathbf{A}^+(\mathbf{Q})=\frac{\partial\mathbf{F}^+(\mathbf{Q})}{\partial\mathbf{Q}},\qquad \mathbf{A}^-(\mathbf{Q})=\frac{\partial\mathbf{F}^-(\mathbf{Q})}{\partial\mathbf{Q}}. \tag{2.14}$$

The Osher-Solomon flux is defined as

$$\mathbf{F}_{i+\frac{1}{2}}(\mathbf{Q}_0,\mathbf{Q}_1)=\mathbf{F}^+(\mathbf{Q}_0)+\mathbf{F}^-(\mathbf{Q}_1). \tag{2.15}$$

In general it is not possible to find functions satisfying (2.13)-(2.14). Nevertheless, for the Euler equations of gas dynamics with ideal equation of state Osher and Solomon proposed expressions involving path dependent integrals in phase-space, as seen below.

From (2.14) we may write the integral relations

$$\int_{\mathbf{Q}_0}^{\mathbf{Q}_1}\mathbf{A}^-(\mathbf{Q})d\mathbf{Q}=\mathbf{F}^-(\mathbf{Q}_1)-\mathbf{F}^-(\mathbf{Q}_0) \tag{2.16}$$

and

$$\int_{\mathbf{Q}_0}^{\mathbf{Q}_1}\mathbf{A}^+(\mathbf{Q})d\mathbf{Q}=\mathbf{F}^+(\mathbf{Q}_1)-\mathbf{F}^+(\mathbf{Q}_0). \tag{2.17}$$

Then we can express (2.15) in three different forms, namely

$$\mathbf{F}_{i+\frac{1}{2}}=\mathbf{F}(\mathbf{Q}_0)+\int_{\mathbf{Q}_0}^{\mathbf{Q}_1}\mathbf{A}^-(\mathbf{Q})d\mathbf{Q}, \tag{2.18a}$$

$$\mathbf{F}_{i+\frac{1}{2}}=\mathbf{F}(\mathbf{Q}_1)-\int_{\mathbf{Q}_0}^{\mathbf{Q}_1}\mathbf{A}^+(\mathbf{Q})d\mathbf{Q}, \tag{2.18b}$$

and

$$\mathbf{F}_{i+\frac{1}{2}}=\frac{1}{2}\big(\mathbf{F}(\mathbf{Q}_0)+\mathbf{F}(\mathbf{Q}_1)\big)-\frac{1}{2}\int_{\mathbf{Q}_0}^{\mathbf{Q}_1}|\mathbf{A}(\mathbf{Q})|d\mathbf{Q}. \tag{2.19}$$

To obtain (2.18a), for example, we use (2.13) to write

$$\mathbf{F}(\mathbf{Q}_0)=\mathbf{F}^+(\mathbf{Q}_0)+\mathbf{F}^-(\mathbf{Q}_0).$$

Then, writing (2.15) as

$$\mathbf{F}_{i+\frac{1}{2}}=\mathbf{F}^+(\mathbf{Q}_0)+\mathbf{F}^-(\mathbf{Q}_1)+\mathbf{F}(\mathbf{Q}_0)-\mathbf{F}(\mathbf{Q}_0)$$

and using (2.17) expression (2.18a) follows.

To obtain the numerical flux from any of the formulae (2.18a)-(2.19) requires the evaluation of the integrals in phase-space. However these integrals depend on the integration path chosen. The Osher-Solomon approach is to select particular integration paths *so as to make the actual integration tractable*.

A distinguishing feature of the Osher-Solomon solver results from choosing a path $I(\mathbf{Q})$ connecting $\mathbf{Q}_0$ to $\mathbf{Q}_1$ as the union of disjoint *partial* paths $I_k(\mathbf{Q})$, for $k=1,\cdots,m$. One way to do this is to associate $I_k(\mathbf{Q})$ to the characteristic field with eigenvalue $\lambda_k(\mathbf{Q})$ and right eigenvector $\mathbf{R}_k(\mathbf{Q})$. $I_k(\mathbf{Q})$ is chosen to connect the states $\mathbf{Q}_{(k-1)/m}$ and $\mathbf{Q}_{k/m}$ and to be tangential to $\mathbf{R}_k(\mathbf{Q})$. Using the parametrization $\mathbf{q}(\xi)$ we write

$$\left.\begin{aligned}&\frac{d\mathbf{q}(\xi)}{d\xi}=\mathbf{R}_k(\mathbf{q}(\xi)),\\&\mathbf{q}(0)=\mathbf{Q}_{\frac{(k-1)}{m}},\qquad \mathbf{q}(\xi_k)=\mathbf{Q}_{\frac{k}{m}}.\end{aligned}\right\} \tag{2.20}$$

The second feature of the Osher-Solomon scheme is that the states $\mathbf{Q}_{k/m}$ are assumed to be known. Osher and Solomon find these states by solving the conventional Riemann problem approximately under the assumption of an all-simple wave pattern in the solution. Under such assumption the integration is performed exactly. Applying a change of variables we may then write

$$\int_{\mathbf{Q}_{\frac{(k-1)}{m}}}^{\mathbf{Q}_{\frac{k}{m}}}\mathbf{A}^-(\mathbf{Q})d\mathbf{Q}=\int_0^{\xi_k}\frac{\partial\mathbf{F}(\mathbf{q}(\xi))}{\partial\mathbf{q}}\frac{d\mathbf{q}(\xi)}{d\xi}d\xi=\int_0^{\xi_k}\lambda_k^-(\mathbf{q})\mathbf{R}_k(\mathbf{q})d\xi. \tag{2.21}$$

If for example, $\lambda_k^-(\mathbf{q})$ is constant along $I_k(\mathbf{q})$, as for a contact discontinuity, then

$$\int_{\mathbf{Q}_{\frac{(k-1)}{m}}}^{\mathbf{Q}_{\frac{k}{m}}}\mathbf{A}^-(\mathbf{Q})d\mathbf{Q}=\begin{cases}0, & \text{if } \lambda_k(\mathbf{q})>0,\\ \mathbf{F}\big(\mathbf{Q}_{\frac{k}{m}}\big)-\mathbf{F}\big(\mathbf{Q}_{\frac{(k-1)}{m}}\big), & \text{if } \lambda_k(\mathbf{q})<0.\end{cases} \tag{2.22}$$

If the path is associated with a genuinely non-linear field then care is required in splitting the path in two parts by a *sonic point*. This implies the additional burden of finding the corresponding *sonic state* $\mathbf{Q}_{sk}$. In the Osher-Solomon approach this task is performed in a

similar manner to that for finding the intermediate states $\mathbf{Q}_{k/m}$. For the one-dimensional Euler equations the complete scheme results in 16 cases, usually displayed in a 4×4 table. For the compressible Euler equations for ideal gases see [43] for full details, for the shallow water equations see [42].

As seen in this section, the Osher-Solomon approximate solver is rather cumbersome and computationally expensive. This, in spite of its attractive features, has prevented its application to a wider variety of hyperbolic systems. In the next section we describe a fully numerical version of the Osher-Solomon scheme that overcomes its complexity, retains its good features and makes it applicable to any hyperbolic system.

3 Towards universal Osher-Type methods

As detailed in the previous section, the original Riemann solver of Osher-Solomon [31] is constructed on the basis of the general definition (2.19), where we now explicitly introduce the integration path in phase-space:

$$\mathbf{F}_{i+\frac{1}{2}}=\frac{1}{2}\big(\mathbf{F}(\mathbf{Q}_0)+\mathbf{F}(\mathbf{Q}_1)\big)-\frac{1}{2}\Big(\int_0^1\big|\mathbf{A}(\mathbf{\Psi}(s))\big|\frac{\partial\mathbf{\Psi}}{\partial s}ds\Big), \tag{3.1}$$

where $\mathbf{\Psi}(s)$ is the *path* that links the left state $\mathbf{Q}_0$ and the right state $\mathbf{Q}_1$ in phase-space. $\mathbf{\Psi}(s)$ is a Lipschitz continuous function with $\mathbf{\Psi}(0)=\mathbf{Q}_0$ and $\mathbf{\Psi}(1)=\mathbf{Q}_1$. Throughout this entire article we will always choose the simple straight-line segment path

$$\mathbf{\Psi}(s)=\mathbf{Q}_0+s\big(\mathbf{Q}_1-\mathbf{Q}_0\big),\quad\text{with }\ 0\le s\le1, \tag{3.2}$$

to connect the two states. With this path the Osher interface flux according to (3.1) is defined by

$$\mathbf{F}_{i+\frac{1}{2}}=\frac{1}{2}\big(\mathbf{F}(\mathbf{Q}_0)+\mathbf{F}(\mathbf{Q}_1)\big)-\frac{1}{2}\Big(\int_0^1\big|\mathbf{A}(\mathbf{\Psi}(s))\big|ds\Big)(\mathbf{Q}_1-\mathbf{Q}_0), \tag{3.3}$$

which makes it very similar to the Roe method [35], that can be also defined in a weak, integral manner according to [5, 32, 48] and that with the use of the segment path (3.2) finally becomes

$$\mathbf{F}_{i+\frac{1}{2}}=\frac{1}{2}\big(\mathbf{F}(\mathbf{Q}_0)+\mathbf{F}(\mathbf{Q}_1)\big)-\frac{1}{2}\Big|\int_0^1\mathbf{A}(\mathbf{\Psi}(s))ds\Big|\big(\mathbf{Q}_1-\mathbf{Q}_0\big). \tag{3.4}$$

Note that the only difference between (3.3) and (3.4) is that the matrix absolute value operator and the integration operator are exchanged. It also follows trivially that for linear hyperbolic systems with constant coefficient matrix $\mathbf{A}$ both schemes are identical and also coincide with the Godunov flux based on the exact Riemann solver.

The main problem with the general definitions (3.3) and (3.4) is actually to compute these integrals for a given hyperbolic system, where the absolute value operator of the Jacobian may lead to very complicated expressions that are either very difficult or even

impossible to integrate analytically. We note that even for the rather simple system of the Euler equations of compressible gas dynamics with ideal equation of state, the Osher flux based on the original definition (3.1) leads to a very cumbersome numerical scheme, see [43] for details and problems. To avoid this cumbersome analytical integration completely, we propose to evaluate the integral (3.3) *numerically* along the segment path with a Gauss-Legendre quadrature rule of sufficient accuracy. Given such a Gaussian rule with G points s_j and associated weights ω_j in the unit interval $I=[0;1]$, we obtain for our generalized Osher flux the following expression:

$$\mathbf{F}_{i+\frac{1}{2}}=\frac{1}{2}\big(\mathbf{F}(\mathbf{Q}_0)+\mathbf{F}(\mathbf{Q}_1)\big)-\frac{1}{2}\Big(\sum_{j=1}^{G}\omega_j\big|\mathbf{A}(\mathbf{\Psi}(s_j))\big|\Big)\big(\mathbf{Q}_1-\mathbf{Q}_0\big). \tag{3.5}$$

Since the domain of definition Ω_q is supposed to be convex and the path is a straight line segment, it is guaranteed that all the intermediate states on the path, $\mathbf{\Psi}(s_j)$, also lie in the domain of definition Ω_q. Furthermore, the system is hyperbolic for all states $Q\in\Omega_q$ and thus also the matrix $\mathbf{A}(\mathbf{\Psi}(s_j))$ is always hyperbolic for all intermediate points. This is a very important property of the scheme (3.5). For the Roe scheme (3.6) we get with the same strategy

$$\mathbf{F}_{i+\frac{1}{2}}=\frac{1}{2}\big(\mathbf{F}(\mathbf{Q}_0)+\mathbf{F}(\mathbf{Q}_1)\big)-\frac{1}{2}\Big|\Big(\sum_{j=1}^{G}\omega_j\mathbf{A}(\mathbf{\Psi}(s_j))\Big)\Big|\big(\mathbf{Q}_1-\mathbf{Q}_0\big). \tag{3.6}$$

Here, in contrast to the generalized Osher flux (3.5), it is *not* automatically guaranteed that the matrix $(\sum_{j=1}^{G}\omega_j\mathbf{A}(\mathbf{\Psi}(s_j)))$ that results from the numerical quadrature process is always hyperbolic. Furthermore, the computation of the eigenstructure is in general more complicated for (3.6) than for (3.5) since in the case of the Osher scheme one can directly use the (known) eigenstructure of the underlying hyperbolic system in each Gaussian quadrature point, whereas for the Roe-type scheme (3.6) one has to compute the eigenstructure of the matrix resulting from the integration process, which is not necessarily similar to the original Jacobian matrix $\mathbf{A}(\mathbf{Q})$ of the governing PDE (2.1). On the other hand, the Roe-type scheme (3.6) requires the computation of an eigenstructure only once, whereas the Osher scheme (3.5) requires the eigenstructure in each Gaussian quadrature point. In those rare cases where complex eigenvalues and eigenvectors are encountered in the matrix $(\sum_{j=1}^{G}\omega_j\mathbf{A}(\mathbf{\Psi}(s_j)))$ of the Roe-type scheme (3.6), we locally reduce the scheme to the classical Rusanov flux at the affected element interface. Note that if we use the *midpoint rule* ($s_1=0.5$, $\omega_1=1$), both schemes (3.5) and (3.6) are *identical*.

Finally, we would like to remark that in contrast to the original Osher flux [31], our new generalized formulation (3.5) is *very simple to implement* and yet *completely general*. It works for *any* general nonlinear hyperbolic system. It only requires the choice of an appropriate Gaussian quadrature rule (or an even more sophisticated adaptive numerical integration technique if thought to be necessary) and the knowledge of the full eigenstructure of $\mathbf{A}$. If the eigenstructure is not known analytically, we compute it numerically using, for example, the **RG** subroutine of the EISPACK package.

4 First order results

In this section we present some results obtained with the first order version of our generalized Osher scheme (3.5). The thorough validation of the first order flux is a very important step to assess the accuracy of the new method, before using it as a building block in high order finite volume and discontinuous Galerkin finite element schemes. For comparison, also some results obtained with the generalized Roe method (3.6) are presented. For the Gaussian quadrature, a three-point Gauss-Legendre rule is used, with points s_j and weights ω_j given by

$$s_{1,3}=\frac{1}{2}\mp\frac{\sqrt{15}}{10},\quad s_2=\frac{1}{2},\quad \omega_{1,3}=\frac{5}{18},\quad \omega_2=\frac{8}{18}. \tag{4.1}$$

If not stated otherwise, the Courant number is set in all computations of this section to CFL$=0.9$.

4.1 Burgers equation

In this subsection we solve the well-known Burgers equation

$$u_t+\left(\frac{1}{2}u^2\right)_x=0, \tag{4.2}$$

with initial condition

$$u(x,0)=\begin{cases} -1, & \text{if } x<0,\\ 1, & \text{if } x\geq 0. \end{cases} \tag{4.3}$$

The exact solution of the problem is a *sonic* rarefaction fan

$$u(x,t)=\begin{cases} \text{sign}(t), & \text{if } |x|>t,\\ \dfrac{x}{t}, & \text{if } |x|\leq t, \end{cases} \tag{4.4}$$

i.e., a continuous function, for which Roe's method is known to produce a steady rarefaction shock, which in fact is a weak solution of (4.2) according to the Rankine-Hugoniot conditions, but that violates the second principle of thermodynamics. In contrast, the Osher scheme is known to be entropy-satisfying and therefore should converge towards the correct entropy solution of the conservation law. The computational results obtained at time $t=0.25$ on a mesh with 100 elements are depicted in Fig. 1, together with the exact solution of the problem. We clearly see how the Roe scheme produces, as expected, an entropy-violating rarefaction shock that is exactly resolved between two grid cells. The original Osher scheme as well as our new Osher-type scheme are entropy satisfying and therefore match very well with the exact solution. Note that a small glitch (in literature also called the *sonic glitch*) is visible for Osher's scheme. However, it gradually disappears with mesh refinement, whereas the rarefaction shock in Roe's scheme does not. For an algebraic proof of the entropy condition for our new Osher-type scheme applied to Burgers equation see Appendix B.

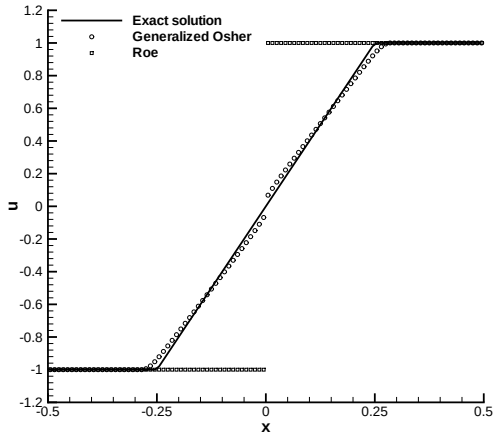

Figure 1: Burgers equation. First order solutions obtained at $t=0.25$ with the generalized Osher scheme (3.5) and Roe's method [35]. The exact solution is also shown.

4.2 Euler equations of compressible gas dynamics

In this section we solve the Euler equations of compressible gasdynamics

$$\frac{\partial}{\partial t}\begin{pmatrix}\rho\\ \rho u\\ \rho E\end{pmatrix}+\frac{\partial}{\partial x}\begin{pmatrix}\rho u\\ \rho u^2+p\\ u(\rho E+p)\end{pmatrix}=0, \tag{4.5}$$

closed by the ideal gas equation of state (EOS)

$$p=(\gamma-1)\Big(\rho E-\frac{1}{2}\rho u^2\Big), \tag{4.6}$$

where γ is the ratio of specific heats and is set to $\gamma=1.4$ in this section. Here, ρ denotes the density, u the velocity, ρE the total energy and p the pressure. We solve a well-known set of shock-tube problems given and explained in detail in [43]. The initial conditions of the shock tube problems are all of the type

$$\mathbf{Q}(x,0)=\begin{cases}\mathbf{Q}_L, & \text{if } x<x_d,\\ \mathbf{Q}_R, & \text{if } x\geq x_d,\end{cases} \tag{4.7}$$

and the initial states left and right are summarized in Table 1. The computational domain is $\Omega=[-1/2,1/2]$ and is discretized with 100 equidistant cells. In Fig. 2 we present the exact solution of Riemann problems RP1-RP6 together with the computational results obtained with the new generalized Osher flux (3.5). For comparison, we also plot the numerical solution obtained with the generalized Roe flux (3.6) based on numerical quadrature of the path-integral as well as the standard Rusanov flux

$$\mathbf{F}_{i+\frac{1}{2}}=\frac{1}{2}\big(\mathbf{F}(\mathbf{Q}_1)+\mathbf{F}(\mathbf{Q}_0)\big)-\frac{1}{2}s_{\max}(\mathbf{Q}_1-\mathbf{Q}_0), \tag{4.8a}$$

$$s_{\max}=\max\big\{|\lambda_i((\mathbf{Q}_1))|,|\lambda_i((\mathbf{Q}_0))|\big\}, \tag{4.8b}$$

Table 1: Initial states left and right for the density ρ, velocity u and the pressure p for the compressible Euler equations. The final output times, (t_{end}) and the initial position of the discontinuity (x_d) are also given.

Case	ρ_L	u_L	p_L	ρ_R	u_R	p_R	t_{end}	x_d
RP1	1.0	0.0	1.0	0.1	0.0	1.0	0.2	0.0
RP2	1.0	0.75	1.0	0.125	0.0	0.1	0.2	-0.1
RP3	1.0	0.0	1000	1.0	0.0	0.01	0.012	0.1
RP4	5.99924	19.5975	460.894	5.99242	-6.19633	46.095	0.035	-0.2
RP5	1.0	-19.59745	1000.0	1.0	-19.59745	0.01	0.012	0.3
RP6	1.0	2.0	0.1	1.0	-2.0	0.1	0.8	0.0

where $s_{\max}$ denotes the maximum of the signal speeds encountered in the left and right states, respectively. In literature, the Rusanov flux (4.8) is also frequently called the local Lax-Friedrichs flux. For all test cases we note that the new generalized Osher flux is robust, even for RP5, where the original method of Osher fails, see [43] for a detailed discussion. As expected, Roe's method produces a significant *sonic glitch* for RP2, which does not disappear with mesh refinement. In contrast, the small glitch present in the Osher method (and that would be even present in the Godunov flux based on the exact Riemann solver) disappears with mesh refinement. Without showing detailed results to save space we would like to note that for the Euler equations of compressible gas dynamics, the results obtained with the HLLC solver [46] and the HLLEM solver [17] are very similar to the ones obtained with the new Osher-type scheme, since for this particular PDE system all of these Riemann solvers are complete. However, it is important to underline that for more general and for more complex PDE systems it is not straightforward to construct HLLC or HLLEM type schemes, while our new Osher-type Riemann solver always takes into account all intermediate waves and extends to any system of hyperbolic conservation laws in a straightforward manner.

4.3 Ideal classical MHD equations

In this section we solve the equations of classical, ideal magnetohydrodynamics (MHD). The augmented PDE system including the hyperbolic divergence-correction term proposed by Dedner et al. [6] reads

$$\frac{\partial}{\partial t}\begin{pmatrix}\rho\\ \rho\vec{v}\\ \rho E\\ \vec{B}\\ \psi\end{pmatrix}+\nabla\cdot\begin{pmatrix}\rho\vec{v}\\ \rho\vec{v}\vec{v}+p_m\mathbf{I}-\frac{1}{4\pi}\vec{B}\vec{B}\\ \vec{v}(\rho E+p_m)-\frac{1}{4\pi}\vec{B}(\vec{v}\cdot\vec{B})\\ \vec{v}\vec{B}-\vec{B}\vec{v}+\psi\mathbf{I}\\ c_h^2\vec{B}\end{pmatrix}=0, \tag{4.9}$$

with

$$p=(\gamma-1)\Big(\rho E-\frac{1}{2}\rho\vec{v}^2-\frac{1}{8\pi}\vec{B}^2\Big),\qquad p_m=p+\frac{1}{8\pi}\vec{B}^2. \tag{4.10}$$

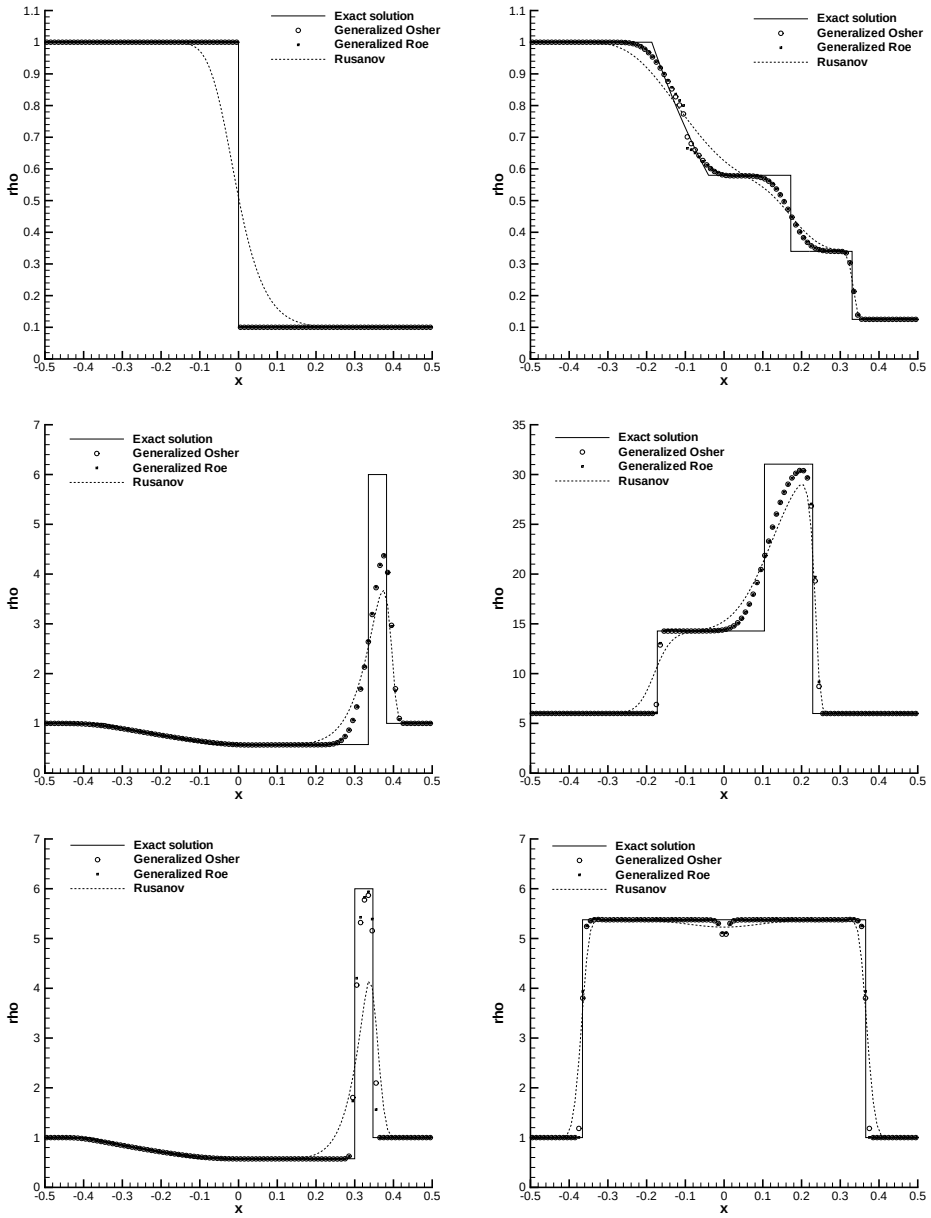

Figure 2: Riemann problems RP1-RP6 for the Euler equations of compressible gas dynamics. First order results for the density ρ, obtained on 100 equidistant cells, are shown.

Here, ρ is the gas density, $\vec{v}=(u,v,w)$ is the velocity vector, $\vec{B}=(B_x,B_y,B_z)$ is the vector of the magnetic field, p is the gas pressure, p_m is the sum of the gas and the magnetic pressure, ρE is the total energy and γ is the ratio of specific heats. $\mathbf{I}$ is the unit matrix and the notation $\vec{x}_1\vec{x}_2$ denotes the dyadic product of two vectors $\vec{x}_1$ and $\vec{x}_2$. The scalar ψ is

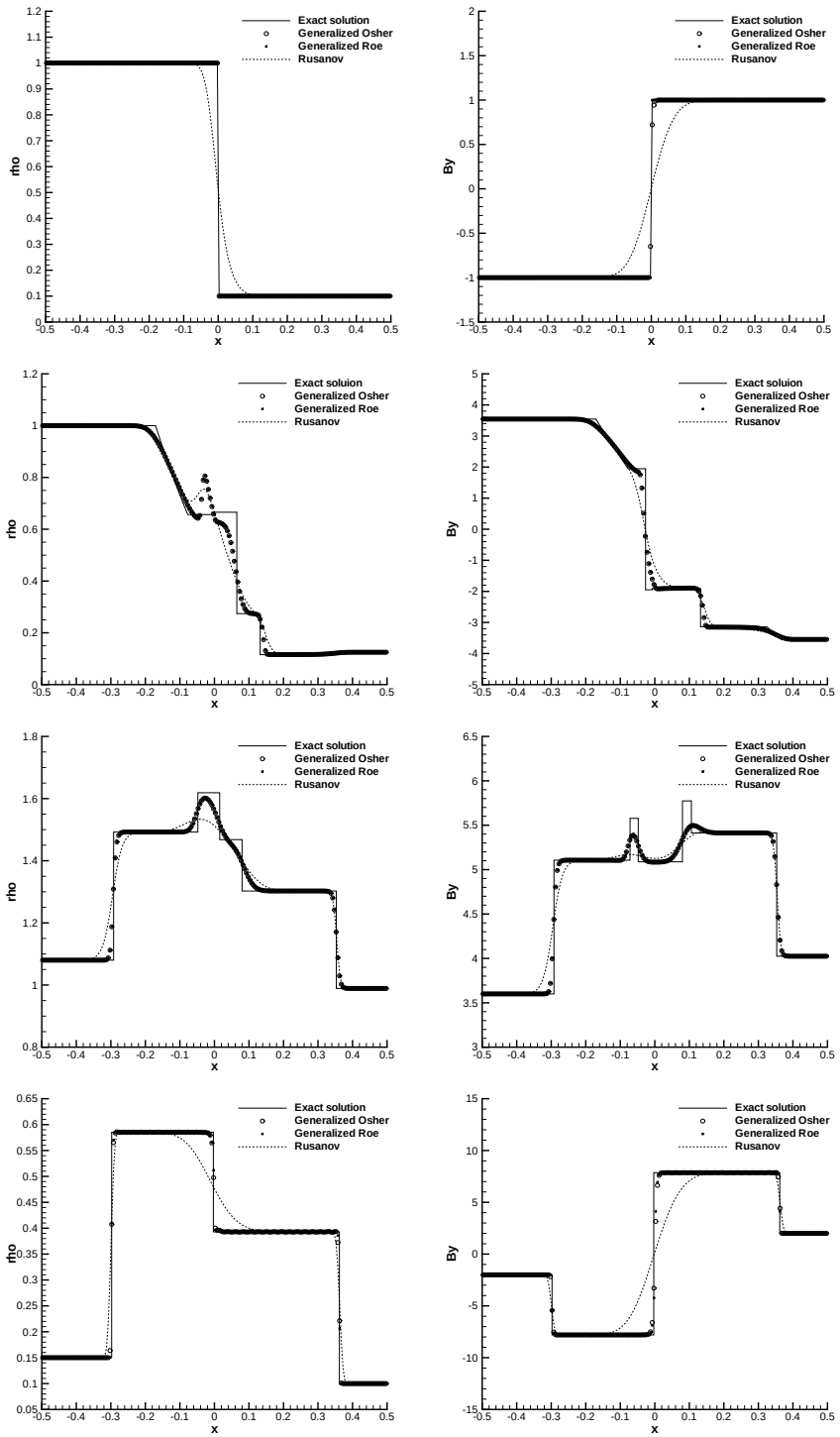

Figure 3: Riemann problems RP1-RP4 for the ideal classical MHD equations.

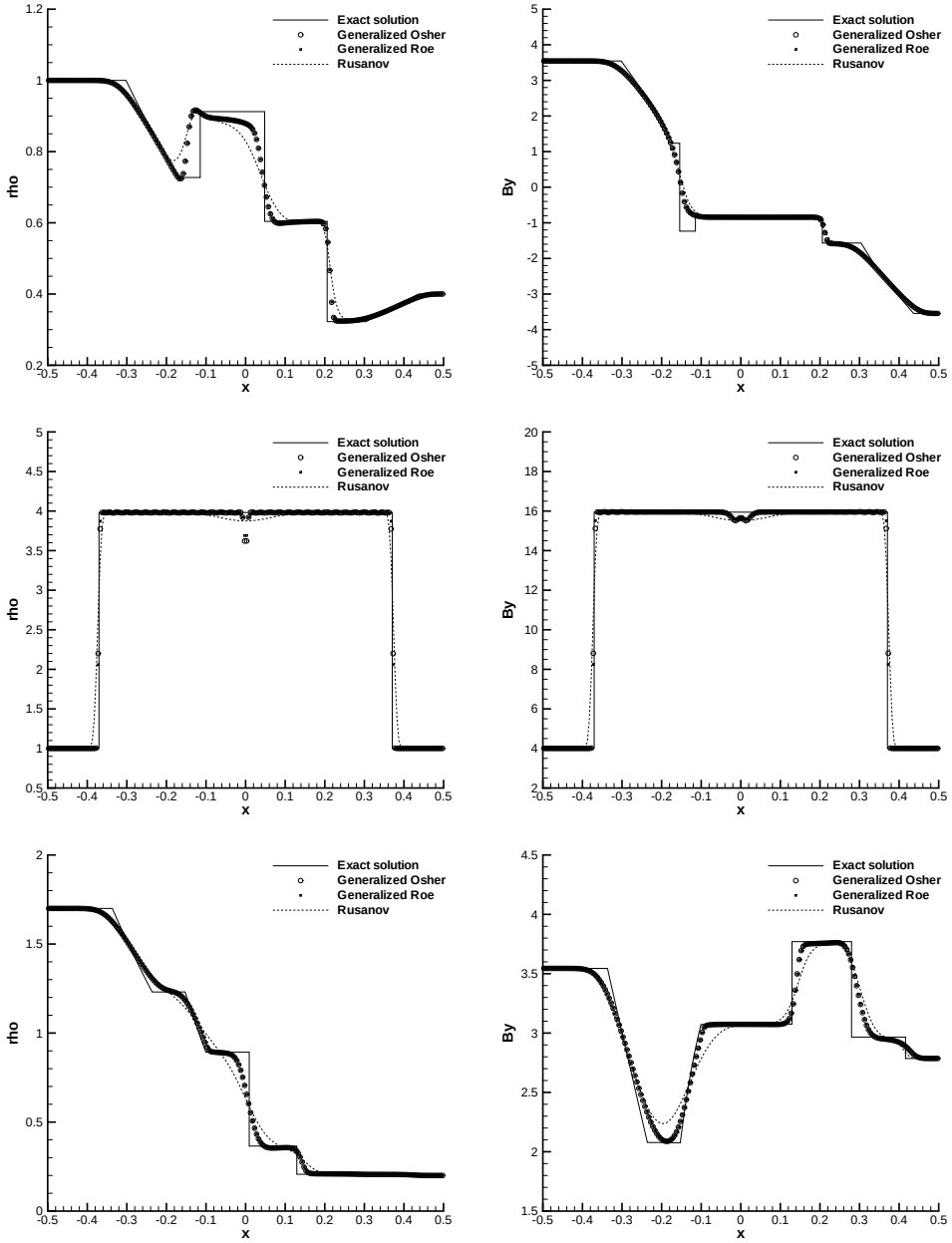

Figure 4: Riemann problems RP5-RP7 for the ideal classical MHD equations.

used for divergence cleaning, see [6], to satisfy the constraint $\nabla\cdot\vec{B}=0$ in multiple space dimensions. In one dimension, this constraint simply reduces to $\partial B_x/\partial x=0$.

To our knowledge, an Osher-Solomon-type flux has never been devised before in literature for the system of MHD equations (4.9). With our general formulation (3.5),

Table 2: Initial states left and right for the density ρ, velocity vector $\vec{v}=(u,v,w)$, the pressure p and the magnetic field vector $\vec{B}=(B_x,B_y,B_z)$ for the ideal classical MHD equations. The final output times, (t_{end}) and the initial position of the discontinuity (x_d) are also given.

Case	ρ	u	v	w	p	B_x	B_y	B_z	t_{end}, x_d
RP1a L:	1.0	0.0	0.0	0.0	1.0	1.0	0.0	0.0	0.1
R:	0.1	0.0	0.0	0.0	1.0	1.0	0.0	0.0	0.0
RP1b L:	$\frac{1}{4\pi}$	1.0	-1.0	0.0	1.0	1.0	-1.0	0.0	0.1
R:	$\frac{1}{4\pi}$	1.0	1.0	0.0	1.0	1.0	1.0	0.0	0.0
RP2 L:	1.0	0.0	0.0	0.0	1.0	$\frac{3}{4}\sqrt{4\pi}$	$\sqrt{4\pi}$	0.0	0.1
R:	0.125	0.0	0.0	0.0	0.1	$\frac{3}{4}\sqrt{4\pi}$	$-\sqrt{4\pi}$	0.0	0.0
RP3 L:	1.08	1.2	0.01	0.5	0.95	2.0	3.6	2.0	0.2
R:	0.9891	-0.0131	0.0269	0.010037	0.97159	2.0	4.0244	2.0026	-0.1
RP4 L:	0.15	21.55	1.0	1.0	0.28	0.05	-2.0	-1.0	0.04
R:	0.1	-26.45	0.0	0.0	0.1	0.05	2.0	1.0	0.0
RP5 L:	1.0	0.0	0.0	0.0	1.0	$1.3\sqrt{4\pi}$	$\sqrt{4\pi}$	0.0	0.16
R:	0.4	0.0	0.0	0.0	0.4	$1.3\sqrt{4\pi}$	$-\sqrt{4\pi}$	0.0	0.0
RP6 L:	1.0	36.87	-0.115	-0.0386	1.0	4.0	4.0	1.0	0.03
R:	1.0	-36.87	0.0	0.0	1.0	4.0	4.0	1.0	0.0
RP7 L:	1.7	0.0	0.0	0.0	1.7	3.899398	3.544908	0.0	0.15
R:	0.2	0.0	0.0	-1.496891	0.2	3.899398	2.785898	2.192064	-0.1

however, the flux follows very naturally once the eigenstructure of the system is known. For the MHD equations, the analytical eigenstructure has been published in the seminal paper of Balsara and Roe [36], hence our generalized Osher flux formulation (3.5) is immediately available for this system. The initial conditions for the shock tube problems are listed in Table 2 and the ratio of specific heats is $\gamma=5/3$ for all cases apart for RP1a, RP1b and RP2, where it is $\gamma=1.4$. We solve all shock-tube problems on a mesh of 200 equidistant cells. The computational results obtained with the first order version of our generalized Osher flux (3.5) and the Roe flux (3.6) based on numerical quadrature of the path integral are depicted in Figs. 3 and 4, together with the exact solution. The Riemann problem RP1a consists in a steady contact wave and problem RP1b consists of an isolated steady Alfvén wave, which is almost perfectly well captured with both, the generalized Osher scheme (3.5) and the Roe-type flux (3.6). This result is expected, since both methods are *complete* Riemann solvers that take into account *all* the waves present in the PDE system. The exact Riemann solver for MHD has kindly been provided by S.A.E.G. Falle [18]. For an alternative exact Riemann solver of the MHD equations, see also [47]. For comparison purposes, we also show the results obtained by the classical Rusanov (local Lax-Friedrichs) flux (4.8). As expected, the resolution of the wave structure obtained with the generalized Osher flux (3.5) and the Roe-type scheme (3.6) is far superior to the one obtained with the simple Rusanov flux. However, only very little differences are visible between the solutions obtained with the generalized Osher scheme (3.5) and the Roe-type flux (3.6), since both methods are *complete* Riemann solvers that account for all the waves present in the Riemann problem.

4.4 Ideal relativistic MHD equations (RMHD)

The ideal relativistic MHD equations (RMHD) form a particularly challenging nonlinear hyperbolic PDE system, since they have the additional difficulty with respect to the previous PDE that the primitive variables needed for expressing the flux $\mathbf{F}(\mathbf{Q})$ can *not* be expressed analytically in terms of the conserved quantities $\mathbf{Q}$. Instead, iterative procedures are necessary to compute $\mathbf{F}(\mathbf{Q})$ for a given state vector $\mathbf{Q}$. The RMHD system reads

$$\frac{\partial \mathbf{Q}}{\partial t}+\nabla\cdot\mathbf{F}(\mathbf{Q})=0, \tag{4.11}$$

with the vector of conserved quantities

$$\mathbf{Q}=\begin{pmatrix} D \\ \vec{M} \\ E \\ \vec{B} \\ \psi \end{pmatrix}=\begin{pmatrix} \gamma\rho \\ \gamma w_{\rm tot}\vec{v}-b^0\vec{b} \\ \gamma^2 w_{\rm tot}-b^0b^0-p_{\rm tot} \\ \vec{B} \\ \psi \end{pmatrix}, \tag{4.12}$$

and the flux tensor

$$\mathbf{F}(\mathbf{Q})=\begin{pmatrix} \gamma\rho\vec{v} \\ \gamma^2 w_{\rm tot}\vec{v}\vec{v}-\vec{v}\vec{b}+p_{\rm tot}\mathbf{I} \\ \gamma^2 w_{\rm tot}\vec{v}-b^0\vec{b} \\ \vec{v}\vec{B}-\vec{B}\vec{v}+\psi\mathbf{I} \\ c_h^2\vec{B} \end{pmatrix}. \tag{4.13}$$

The equation of state is

$$e=\rho+\frac{p}{\Gamma-1}, \tag{4.14}$$

the Lorentz factor, denoted as γ in this section, is defined by

$$\gamma=\frac{1}{\sqrt{1-\vec{v}^2}}, \tag{4.15}$$

further quantities appearing in (4.12) and (4.13) are given by

$$b^0=\gamma\vec{v}\cdot\vec{B}, \qquad \vec{b}=\frac{\vec{B}}{\gamma}+\gamma\vec{v}, \qquad |b|^2=\frac{\vec{B}^2}{\gamma^2}+(v_kB_k)^2, \tag{4.16}$$

from which total enthalpy and total pressure are then finally defined as

$$w_{\rm tot}=e+p+|b|^2, \qquad p_{\rm tot}=p+\frac{1}{2}|b|^2. \tag{4.17}$$

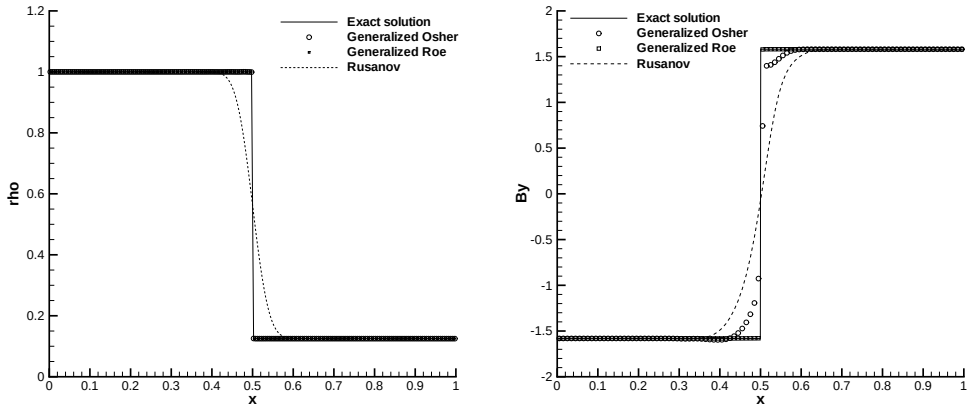

Figure 5: Riemann problem RP0a (steady contact wave, left) and Riemann problem RP0b (steady Alfvén wave, right) for the relativistic MHD equations (RMHD).

In this entire section, the speed of light is supposed to be set to unity. The computation of the primitive variables ρ, $\vec{v}$ and p from the vector $\mathbf{Q}$ of conserved quantities is very complicated. It can not be done analytically but requires necessarily the use of an iterative technique, such as Newton's method. A very elegant, robust and efficient way of transforming the conservative variables to primitive variables using the analytic inversion of a third degree polynomial together with the solution of a single nonlinear scalar equation is given in [51]. More details about this very interesting hyperbolic system can be found in [1, 9, 19, 26, 34, 51]. The exact solution of the Riemann problem has been published in [19, 34] and the eigenstructure has been made available in [1]. This allows us immediately to apply the generalized Osher flux (3.5) to the rather complicated system (4.11)-(4.13). We start with the assessment of the ability of the two Riemann solvers (3.5) and (3.6) whether they conserve exactly stationary contact (RP0a) and Alfvén (RP0b) waves. The results are depicted in Fig. 5 and we find that both schemes preserve steady contact waves for this system but that *only* the generalized Roe flux (3.6) is able to conserve the steady Alfvén wave exactly, whereas the generalized Osher flux adds a significant amount of spurious numerical diffusion. This diffusive behavior is still present even when using more accurate and more sophisticated quadrature rules. The RMHD equations are the only system found so far by the authors that poses serious problems in the conservation of steady intermediate waves for the generalized Osher flux in the formulation (3.5) used in this paper. Since our flux is based on the numerical quadrature along the segment path, further investigations about the choice of a more appropriate path will be the topic of future research.

We then solve a series of classical shock tube problems proposed in [1] using both, the generalized Osher flux (3.5) as well as the Roe-type flux (3.6). The exact solution has been very kindly provided by [19, 34]. The results are depicted in 6, where in both cases we note a remarkable improvement with respect to the simple Rusanov flux. In RP2, which contains a *sonic* rarefaction we see that the generalized Osher scheme (3.5) behaves better

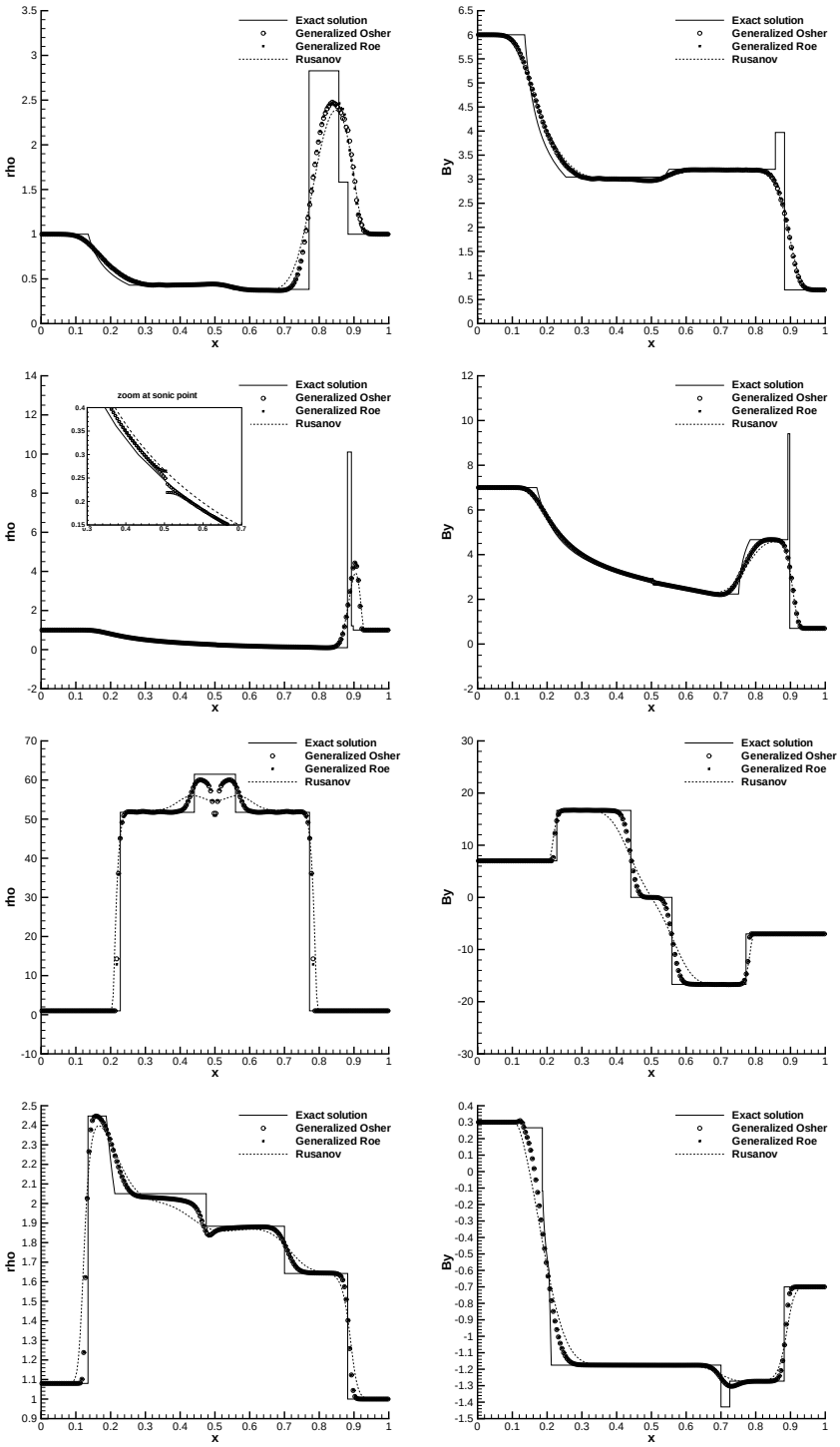

Figure 6: Riemann problems RP1-RP4 for the relativistic MHD (RMHD) equations.

Table 3: Initial states left (L) and right (R) for the relativistic RMHD shock tube problems and final times t_e.

Case	ρ	p	u	v	w	B_y	B_z	B_x	t_e
RP0a L:	1.0	1.0	0.0	0.0	0.0	0.0	0.0	0.0	0.2
RP0a R:	0.125	1.0	0.0	0.0	0.0	0.0	0.0	0.0	
RP0b L:	1.0	1.0	-0.5	0.5	0.0	-1.58113883	0.0	1.58113883	0.2
RP0b R:	1.0	1.0	-0.5	-0.5	0.0	1.58113883	0.0	1.58113883	
RP1 L:	1.0	30.0	0.0	0.0	0.0	6.0	6.0	5.0	0.4
RP1 R:	1.0	1.0	0.0	0.0	0.0	0.7	0.7	5.0	
RP2 L:	1.0	1000.0	0.0	0.0	0.0	7.0	7.0	10.0	0.4
RP2 R:	1.0	0.1	0.0	0.0	0.0	0.7	0.7	10.0	
RP3 L:	1.0	0.1	0.999	0.0	0.0	7.0	7.0	10.0	0.4
RP3 R:	1.0	0.1	-0.999	0.0	0.0	-7.0	-7.0	10.0	
RP4 L:	1.08	0.95	0.4	0.3	0.2	0.3	0.3	2.0	0.55
RP4 R:	1.0	1.0	-0.45	-0.2	0.2	-0.7	0.5	2.0	

than the Roe-type method (3.6) and produces a much less pronounced *sonic glitch*, see zoom in Fig. 6.

4.5 The equations of nonlinear elasticity

Here, we consider the equations of nonlinear elasticity (NLE) as derived by Godunov and Romenski in Eulerian coordinates in [21–23]. This very interesting system has been studied numerically for example in [9, 39], where rather simple centered-type numerical fluxes have been used. Exact solutions for the Riemann problem of the nonlinear elasticity equations have first been presented in [2, 39]. In this article we will apply for the first time a *complete* Riemann solver to these complex equations. We mostly follow the notation given in [39], except for the deformation gradient that we call c_{ij} instead of F_{ij}, thus avoiding confusion with the flux tensor of the hyperbolic system. The vector of conservative variables is then $\mathbf{Q}=(\rho,\rho\vec{v},\rho c_{ij},\rho E)^T$ and the flux tensor is defined as

$$\mathbf{F}(\mathbf{Q})=\begin{pmatrix} \rho\vec{v} \\ \rho\vec{v}\vec{v}-\sigma_{ij} \\ \rho c_{ij}\vec{v}-\rho c_{ij}\vec{v} \\ \vec{v}\rho E-\sigma_{ik}\vec{v} \end{pmatrix}. \tag{4.18}$$

Note that according to [39] the equation for density replaces one equation for the deformation gradient, say c_{11}. The total energy is defined as usual as $\rho E=\rho(e+\vec{v}^2/2)$. The stress tensor σ_{ij} is a complicated nonlinear function of the deformation gradient c_{ij} and depends on the equation of state (EOS) that is needed to close the system. The EOS defines the internal energy e as a function of the deformation gradient c_{ij} and entropy S as $e=e(c_{ij},S)$. Then, the following definitions for density ρ, strain tensor g_{ij}, stress tensor σ_{ij}

and temperature T hold:

$$\rho=\frac{\rho_0}{\det c_{ij}},\qquad g_{ij}=c_{ji}^{-1}c_{jk}^{-1},\qquad \sigma_{ik}=\rho c_{ij}\frac{\partial e}{\partial c_{kj}}=-2\rho g_{ij}\frac{\partial e}{\partial g_{jk}},\qquad T=\frac{\partial e}{\partial S}, \tag{4.19}$$

where ρ_0 is the constant density in the reference state. In an isotropic medium, the internal energy e is a function of three invariants of the strain tensor g_{ij}:

$$e(I_1,I_2,I_3)=\frac{K_0}{2\alpha^2}\left(I_3^{\frac{\alpha}{2}}-1\right)^2+c_V T_0 I_3^{\frac{\gamma}{2}}\left(e^{\frac{S}{c_V}}-1\right)+\frac{B_0}{2}I_3^{\frac{\beta}{2}}\left(\frac{1}{3}I_1^2-I_2\right), \tag{4.20}$$

with the invariants

$$I_1=\mathrm{tr}(g_{ij})=g_{11}+g_{22}+g_{33},\quad I_3=\det(g_{ij})=\left(\frac{\rho}{\rho_0}\right)^2, \tag{4.21a}$$

$$I_2=(g_{11}g_{22}-g_{12}g_{21})+(g_{22}g_{33}-g_{23}g_{32})+(g_{33}g_{11}-g_{31}g_{13}). \tag{4.21b}$$

According to [39], K_0 and B_0 are the squared speed of the pressure and the shear wave, respectively, c_V is the heat capacity at constant volume, T_0 is the reference temperature and α, β and γ are constants characterizing the non-linearities in the EOS. We solve two of the one-dimensional shock tube problems proposed in [39] using the new generalized Osher flux (3.5). The material properties for copper are chosen as in [39], i.e., we use $\rho_0=8.9$, $K_0=c_0^2-4b_0^2/3$, $B_0=b_0^2$, $c_0=4.6$, $b_0=2.1$, $T_0=300$ and $c_v=0.4\times10^{-3}$. We use furthermore $\alpha=1$, $\beta=3$ and $\gamma=2$. The shock tube problems are solved on the domain $\Omega=[0;1]$ using only 100 cells. Transmissive boundaries are imposed in x-direction. For this system, we compute the eigenstructure in a fully numerical way using the **RG** subroutine of the EISPACK package. The initial condition consists of two piecewise constant states, separated by a discontinuity at $x=0.5$. The initial states for all test cases are given in terms of the primitive variables in Table 4. The first problem RP0 consists of an isolated, steady contact discontinuity. The complete Riemann solver should conserve it exactly. We note, that in practice this is not the case, due to the errors introduced in the numerical integration process and most likely also due to the errors introduced by the numerical computation of the eigenstructure. However, the resolution is much better than the one obtained with an incomplete Riemann solver. RP1 corresponds to the three-wave shock tube problem

Table 4: Initial states left (L) and right (R) for the shock tube problems solved for the equations of nonlinear elasticity and final output times t_e.

Case	u	v	c_{11}	c_{12}	c_{21}	c_{22}	S	t_e
RP0 L:	0.0	0.0	1.156276	0.034688	0.093191	1.002196	0.001	0.2
RP0 R:	0.0	0.0	1.0	0.03	0.02	1.0	0.0	
RP1 L:	0.0	0.0	0.95	0.0	0.0	1.0	0.001	0.06
RP1 R:	0.0	0.0	1.0	0.0	0.0	1.0	0.0	
RP2 L:	0.0	1.0	0.95	0.0	0.05	1.0	0.001	0.06
RP2 R:	0.0	0.0	1.0	0.0	0.0	1.0	0.0	

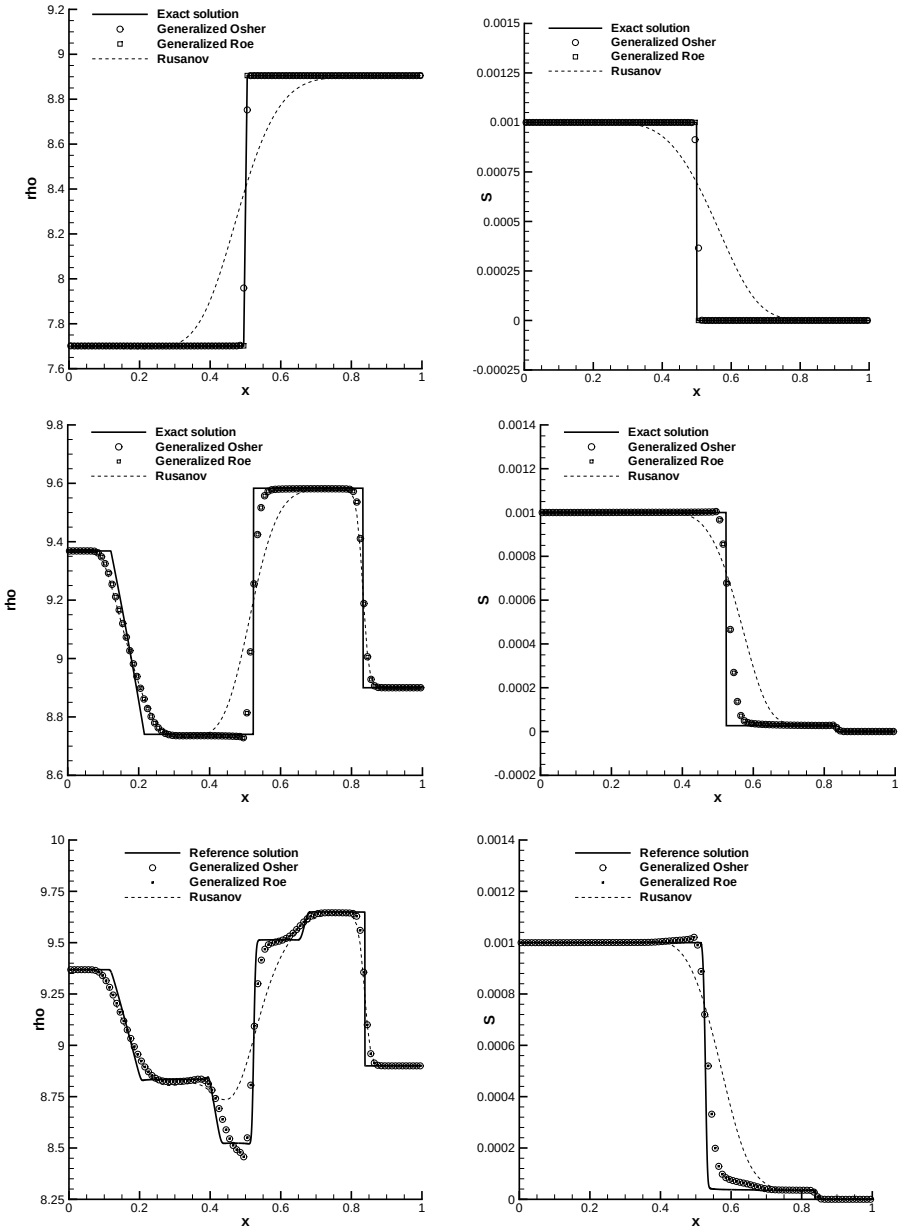

Figure 7: Riemann problems RP0-RP2 for the equations of nonlinear elasticity (top to bottom). RP0 is the stationary contact wave, RP1 contains only three waves and RP2 contains all five waves.

and test case RP2 corresponds to the five-wave shock tube problem described in [39]. The second test case consists of two pieces of material that have been subject to different strain conditions and that are afterwards attached to each other. Dr. Titarev kindly provided us with the exact solution of the three-wave shock tube problem and with the

numerical reference solution of the five-wave shock tube problem, as published in [39]. Our numerical results for all test cases are shown in Fig. 7. As expected, the complete Riemann solver behaves much better than the simple Rusanov flux.

5 Extension to higher order and multiple space dimensions

In this section we use the new Osher flux (3.5) as a building block of high order finite volume and discontinuous Galerkin schemes on unstructured meshes in multiple space dimensions. For this purpose, we use the general framework of P_NP_M method proposed by Dumbser et al. in [9]. To save space, we only recall the basic concept of the P_NP_M method here and refer the interested reader to [7–10, 12] for more details. The hyperbolic conservation laws under consideration here have all the form

$$\frac{\partial \mathbf{Q}}{\partial t}+\nabla\cdot\mathbf{F}(\mathbf{Q})=0. \tag{5.1}$$

The computational domain Ω is discretized by a set of conforming elements T_i, for example triangles in 2D and tetrahedrons in 3D. The numerical solution of (5.1) at the current time t^n is denoted by $u_h^n\in V_h$, where V_h is the space of piecewise polynomials of degree N. Then, we apply a reconstruction procedure to get another numerical approximation for (5.1) that is denoted by $w_h^n\in W_h$, where W_h is the space of piecewise polynomials of degree $M\geq N$. The reconstruction is done by defining a stencil $\mathcal{S}_i$ containing the element T_i and an appropriate set of neighbors of T_i. Before describing the reconstruction procedure, we introduce the following operators:

$$\langle f,g\rangle_{T_i}=\int_{t^n}^{t^{n+1}}\int_{T_i}\big(f(\vec{x},t)\cdot g(\vec{x},t)\big)d\vec{x}dt, \tag{5.2a}$$

$$[f,g]_{T_i}^t=\int_{T_i}\big(f(\vec{x},t)\cdot g(\vec{x},t)\big)d\vec{x}, \tag{5.2b}$$

$$\{f,g\}_{\partial T_i}=\int_{t^n}^{t^{n+1}}\int_{\partial T_i}\big(f(\vec{x},t)\cdot g(\vec{x},t)\big)dSdt, \tag{5.2c}$$

which are the scalar products of two functions f and g over the space-time element $T_i\times[t^n;t^{n+1}]$, the spatial element T_i, and the space-time boundary element $\partial T_i\times[t^n;t^{n+1}]$ respectively.

For the reconstruction step we require a weak identity between the reconstructed solution w_h and the original numerical solution u_h for all elements in the stencil, i.e.,

$$[\phi_k,w_h^n]_{T_j}=[\phi_k,u_h^n]_{T_j},\quad \forall T_j\in\mathcal{S}_i,\quad \phi_k\in V_h. \tag{5.3}$$

Here, ϕ_k is a test function from the space V_h. The reconstruction equations (5.3) are solved using the constrained least-squares method presented in [13], where the linear constraint is given by

$$[\phi_k,w_h^n]_{T_i}=[\phi_k,u_h^n]_{T_i},\quad \phi_k\in V_h, \tag{5.4}$$

i.e., Eq. (5.3) must hold at least *exactly* in the element T_i under consideration. To enforce monotonicity, we use the WENO scheme proposed in [13, 14]. The reconstruction polynomials w_h^n are now evolved *locally* inside each element using the local space-time discontinuous Galerkin approach introduced in [11] and extended to multiple space dimensions in [10, 16]. Multiplying the PDE (5.1) with a test function $\theta_k = \theta_k(\vec{x},t)$ from the space Z_h of space-time polynomials of degree M, integrating the first term with the time derivative by parts in time and introducing the initial condition w_h^n, we get an element-local system for the element-local predictor solution q_h in space-time as follows:

$$\left([\theta_k, q_h]_{T_i}^{t^{n+1}} - \left\langle \frac{\partial}{\partial t}\theta_k, q_h \right\rangle_{T_i} \right) + \left\langle \theta_k, \nabla \cdot F(q_h) \right\rangle_{T_i} = [\theta_k, w_h^n]_{T_i}^{t^n}. \tag{5.5}$$

The resulting element-local nonlinear algebraic system (5.5) can be solved very efficiently using the fixed-point iteration scheme proposed in [7, 9, 16]. The final $P_N P_M$ scheme for the update of the numerical solution u_h^{n+1} to the new time level t^{n+1} reads

$$[\Phi_k, u_h^{n+1}]_{T_i}^{t^{n+1}} - [\Phi_k, u_h^n]_{T_i}^{t^n} - \left\langle \nabla \Phi_k, F(q_h) \right\rangle_{T_i} + \left\{ \Phi_k, \mathcal{G}_{i+\frac{1}{2}}(q_h^-, q_h^+) \cdot \vec{n} \right\}_{\partial T_i} = 0, \tag{5.6}$$

where q_h^- and q_h^+ denote the predictor solution from within the element T_i and from the neighbor element of T_i, respectively. $\mathcal{G}_{i+1/2} \cdot \vec{n}$ is the numerical flux in *normal* direction, so we can solve local Riemann problems in normal direction and hence use the same expression (3.5) as in the one-dimensional case, where the Jacobian $\mathbf{A}$ is understood as the Jacobian of the flux in *normal direction*, i.e., $\mathbf{A} = (\partial \mathbf{F}/\partial \mathbf{Q}) \cdot \vec{n}$. The $P_N P_M$ method is a fully-discrete one-step scheme that can be summarized in the following three simple steps:

1. At the current time level t^n compute the piecewise reconstruction polynomials $w_h^n \in W_h$ of degree M from the original numerical solution $u_h^n \in V_h$ represented by piecewise polynomials of degree N using the reconstruction equations (5.3). We thus have $w_h^n = \mathcal{R}(u_h^n)$, where $\mathcal{R}$ is a shorthand notation for the reconstruction operator.
2. Evolve the reconstruction polynomials w_h^n in time for each element, without taking into account any neighbor information, using the local space-time DG scheme (5.5). The solution is an element-local space-time polynomial $q_h = q_h(\vec{x},t) \in Z_h$, defined on each element T_i for all times $t \in [t^n; t^{n+1}]$. In short notation we have $q_h = \mathcal{E}(w_h^n)$, where $\mathcal{E}$ is an abbreviation for the element-local evolution operator.
3. Update the numerical solution u_h^n to the new time level t^{n+1} using the fully-discrete one-step $P_N P_M$ scheme (5.6), denoted with $u_h^{n+1} = u_h^n + \mathcal{P}_N^M(q_h)$, where the $P_N P_M$ scheme is abbreviated with $\mathcal{P}_N^M$. This yields the numerical solution u_h^{n+1} at the new time level and the algorithm starts again with Step 1.

We note that the $P_N P_M$ scheme (5.6) reduces to the classical finite volume method for $N = 0$ and to the standard discontinuous Galerkin scheme for $N = M$. A new class of methods is obtained for $N \neq 0$ and $M > N$. The one-step time integration procedure using the local space-time DG scheme (5.5) can been seen as a direct extension to higher order of

accuracy of the time-evolution procedure in the MUSCL method of van Leer [50]. It can further be interpreted also as a weak formulation of the Cauchy-Kovalewski procedure used in the original ENO method of Harten et al. [24], in the ADER schemes of Titarev and Toro [40,41] and in the ADER-DG & LW-DG approaches presented in [15,33].

5.1 Numerical convergence study

The convergence studies of the two-dimensional version of our $P_N P_M$ schemes are carried out solving the Euler equations of compressible gas dynamics,

$$\frac{\partial}{\partial t}\begin{pmatrix}\rho\\ \rho\vec{v}\\ \rho E\end{pmatrix}+\nabla\cdot\begin{pmatrix}\rho\vec{v}\\ \rho\vec{v}\vec{v}+p\mathbf{I}\\ \vec{v}(\rho E+p)\end{pmatrix}=0, \tag{5.7}$$

closed again by the ideal gas EOS

$$p=(\gamma-1)\Big[\rho E-\frac{1}{2}\rho(u^2+v^2)\Big]. \tag{5.8}$$

We consider the smooth two-dimensional example of a convected isentropic vortex given for example by Hu and Shu in [27]. The initial condition is a linear superposition of a homogeneous background field and some perturbations δ:

$$(\rho,u,v,p)=\big(1+\delta\rho,1+\delta u,1+\delta v,1+\delta p\big). \tag{5.9}$$

The perturbations of the velocity components u and v as well as the perturbations of entropy $S=p/\rho^\gamma$ and temperature T of the vortex are given by

$$\begin{pmatrix}\delta u\\ \delta v\end{pmatrix}=\frac{\epsilon}{2\pi}e^{\frac{1-r^2}{2}}\begin{pmatrix}-(y-5)\\ (x-5)\end{pmatrix},\qquad \delta S=0,\qquad \delta T=-\frac{(\gamma-1)\epsilon^2}{8\gamma\pi^2}e^{1-r^2}, \tag{5.10}$$

with $r^2=(x-5)^2+(y-5)^2$, the vortex strength $\epsilon=5$ and the ratio of specific heats $\gamma=1.4$. If we define the relationship between density, pressure and static temperature in a nondimensional fashion so that the gas constant becomes equal to unity, we obtain the following perturbations of the primitive variables density and pressure:

$$\delta\rho=(1+\delta T)^{\frac{1}{\gamma-1}}-1,\qquad \delta p=(1+\delta T)^{\frac{\gamma}{\gamma-1}}-1. \tag{5.11}$$

The computational domain is $\Omega=[0;10]\times[0;10]$ and four periodic boundary conditions are imposed. After one period of $t=10$, the exact solution is given by the initial condition (5.9). For measuring the error between the numerical solution u_h and the exact solution u_e, we first apply the reconstruction operator in order to get $w_h=\mathcal{R}(u_h)$ and then we use the continuous L^2-norm

$$\|w_h-u_h\|=\Big(\int_\Omega|w_h-u_e|^2dV\Big)^{\frac{1}{2}}, \tag{5.12}$$

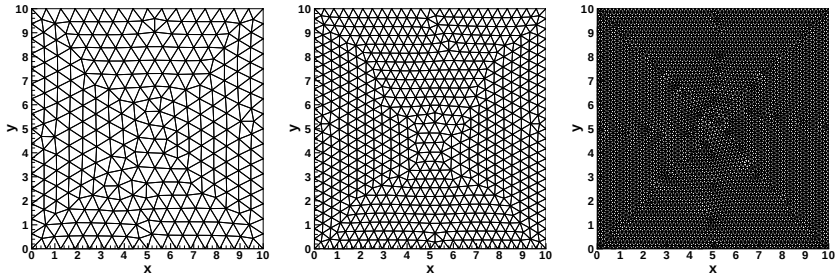

Figure 8: Sequence of triangular meshes used for the numerical convergence studies.

in which the integration is approximated using Gaussian integration formulae with appropriate order of accuracy. We use the sequence of irregular triangular meshes shown in Fig. 8 and apply both, the new generalized Osher flux (3.5) as well as a standard Rusanov method (4.8) for a third order finite volume scheme, that would be a P_0P_2 scheme in the more general P_NP_M framework. The results obtained with the Osher flux and the Rusanov flux are summarized in Table 5 and clearly underline that even for smooth solutions and a third order finite volume scheme, the choice of the numerical flux has still a significant influence. We also report the absolute CPU times in seconds using one CPU core of an Intel Core 2 CPU with 2.5 GHz. We find that on the finest meshes the scheme based on the Osher-type flux is about 60 % slower with about 2.4 times smaller errors compared to the Rusanov-based method. Further convergence results for a selected fourth and sixth order P_NP_M scheme with the generalized Osher flux (3.5) are presented in Table 6, which shows that the designed order of accuracy has been reached very well even for very high order P_NP_M schemes.

Table 5: Convergence results and CPU times for third order finite volume schemes (P_0P_2). The standard Rusanov flux (left) and the new generalized Osher scheme (right). Errors refer to the variable ρ (density).

N_G	L_2	$\mathcal{O}(L_2)$	CPU [s]	L_2	$\mathcal{O}(L_2)$	CPU [s]
P_0P_2	Rusanov			Generalized Osher		
24	1.93E-01		10	9.28E-02		19
32	9.82E-02	2.3	25	4.68E-02	2.4	46
64	1.89E-02	2.4	263	8.41E-03	2.5	385
128	2.79E-03	2.8	2654	1.16E-03	2.9	4233

Table 6: Convergence results for two selected fourth and sixth order P_NP_M schemes using the new generalized Osher scheme. Errors refer to the variable ρ (density).

N_G	L_2	$\mathcal{O}(L_2)$	L_2	$\mathcal{O}(L_2)$
	P_2P_3		P_3P_5	
16	3.79E-03		8.43E-03	
24	7.73E-04	3.9	2.11E-04	5.3
32	2.15E-04	4.4	1.79E-05	6.1
64	1.32E-05	4.0	3.00E-06	6.2

5.2 Euler equations with real gas EOS

In the last section of this paper we show that the generalized Osher flux (3.5) can be even applied to the multi-dimensional Euler equations (5.7) with *real gas* equation of state. Here, we use the very well-known van der Waals model [49] given by

$$(p+\alpha\rho^2)(1-\rho\beta)=\rho RT, \qquad e=c_v T-\alpha\rho, \tag{5.13}$$

that reduces to the ideal gas EOS for $\alpha=\beta=0$. e is the specific internal energy that is linked to the total energy as usual by $\rho E=\rho e+\rho\vec{v}^2/2$. The eigenstructure for the Euler equations (5.7) with general EOS can still be computed analytically, so the generalized Osher flux (3.5) can be applied directly.

5.3 Shock-tube problems

We first solve three shock-tube problems on the domain $\Omega=[0;1]\times[0;0.1]$ with the initial discontinuity located at $x=0.5$ and the initial left and right states given in Table 7. The constants in the van der Waals EOS (5.13) are chosen as $\alpha=0.138$, $\beta=3.258\times10^{-5}$, $R=231.11$ and $c_v=577.8$. The computations are carried out with a P_0P_2 WENO finite volume scheme on an unstructured triangular mesh of characteristic mesh size $h=1/100$. The results are depicted in Figs. 9-11. The results obtained with the generalized Osher flux (3.5) inside the third order WENO finite volume scheme are more accurate compared to the ones obtained with the Rusanov flux (4.8). The exact solution of the Riemann problem has been kindly provided by Dr. C. E. Castro, who intensively studied approximate solvers for the generalized or high-order Riemann problem, see [4].

Table 7: Initial states left and right for the temperature T, velocity $\vec{v}=(u,v)$ and the pressure p for the compressible Euler equations with van der Waals EOS. The final output times, (t_{end}) are also given.

Case	T_L	u_L	v_L	p_L	T_R	u_R	v_R	p_R	t_{end}
RP0	4.0	0.0	0.1	1.0	0.4	0.0	-0.1	1.0	0.01
RP1	0.004439155	-0.6	0.0	1.5	0.01357751	-0.4	0.0	3.0	0.2
RP2	0.004923902	0.0	0.0	1.0	0.00353618	0.0	0.0	0.1	0.2

5.4 Explosion problem

Finally, we solve a circular explosion problem with the initial condition given by

$$\mathbf{Q}(\vec{x},0)=\begin{cases}\mathbf{Q}_L, & \text{if } r<R,\\ \mathbf{Q}_R, & \text{if } r\geq R,\end{cases} \tag{5.14}$$

with $r^2=x^2+y^2$, and the left and right states are taken from the previous Riemann problem RP2. The discontinuity is located at a radius of $R=0.5$ and the computational domain

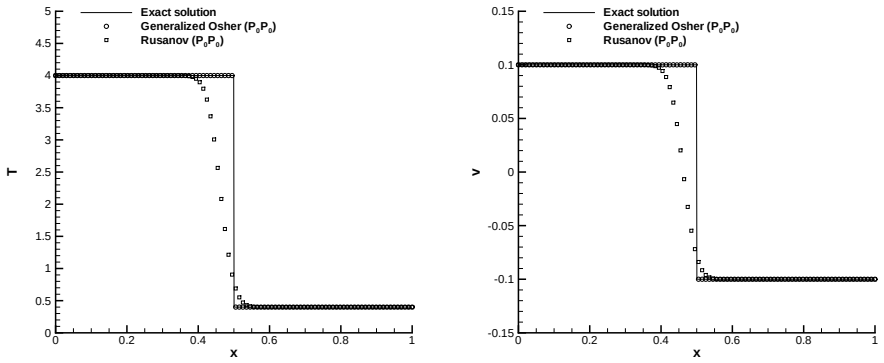

Figure 9: Riemann problem RP0 for the compressible Euler equations with van der Waals EOS. Stationary contact and shear wave.

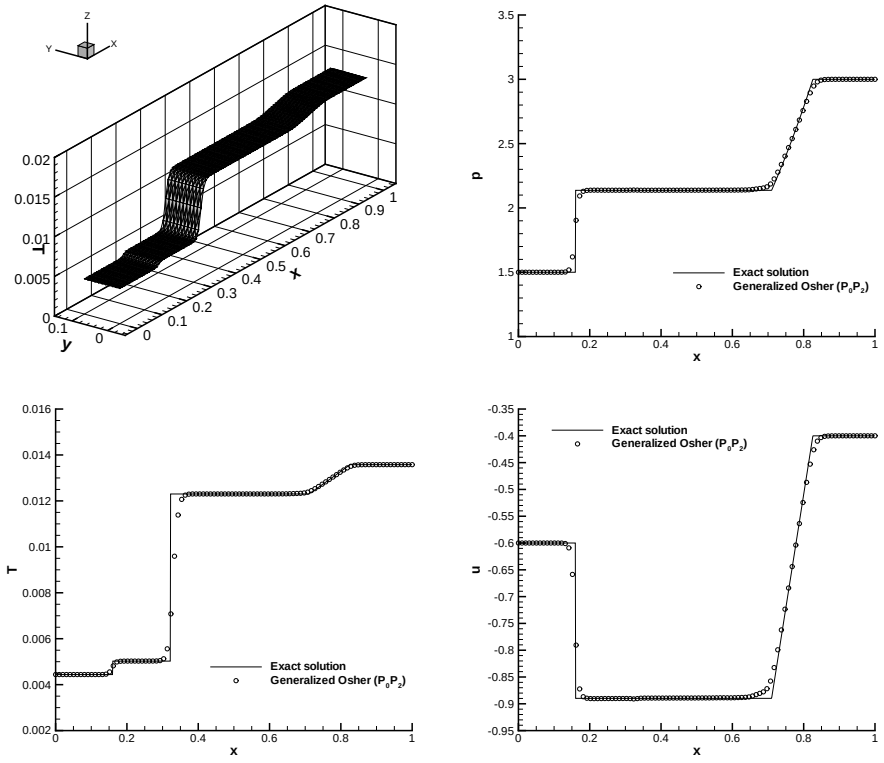

Figure 10: Riemann problem RP1 for the Euler equations with van der Waals EOS.

Ω is a circle with radius one. The triangular mesh used for this computation has a characteristic mesh spacing of $h=1/100$. Since the test case is symmetric in angular direction, a reliable reference solution can be obtained by solving the Euler equations with geometric reaction source terms in one space dimension with a classical second order TVD scheme

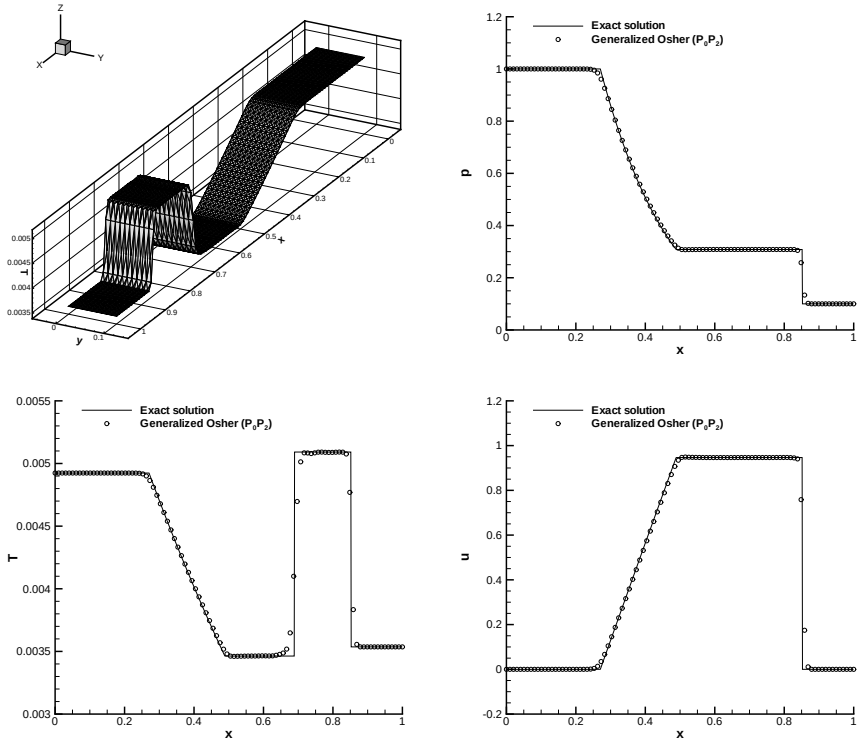

Figure 11: Riemann problem RP2 for the Euler equations with van der Waals EOS.

on a fine mesh with 25000 cells, see [43] for more details. The results are shown in Fig. 12 and we note an excellent agreement between the numerical solution obtained with the new Osher flux and the third order WENO finite volume scheme on the two-dimensional unstructured mesh and the one-dimensional reference solution.

6 Conclusions

We have presented a simple and efficient generalization of the Osher-Solomon flux [31] to general nonlinear hyperbolic systems by evaluating the path integral along a straight line segment in phase-space in a purely numerical way with a simple Gauss-Legendre quadrature formula. The only requirement for the application of our formulation (3.5) is the knowledge of the full eigenstructure of the system. If it is not known analytically, it can also be computed numerically. We have shown first order results for the Euler equations of compressible gas dynamics, the classical and relativistic MHD equations as well as for the equations of nonlinear elasticity. Our scheme is a *complete* Riemann solver that takes into account all the waves, but it is nevertheless very *simple* to implement.

It can also be directly used as a building block for high order finite volume and discontinuous Galerkin finite element schemes in multiple space dimensions, as shown in

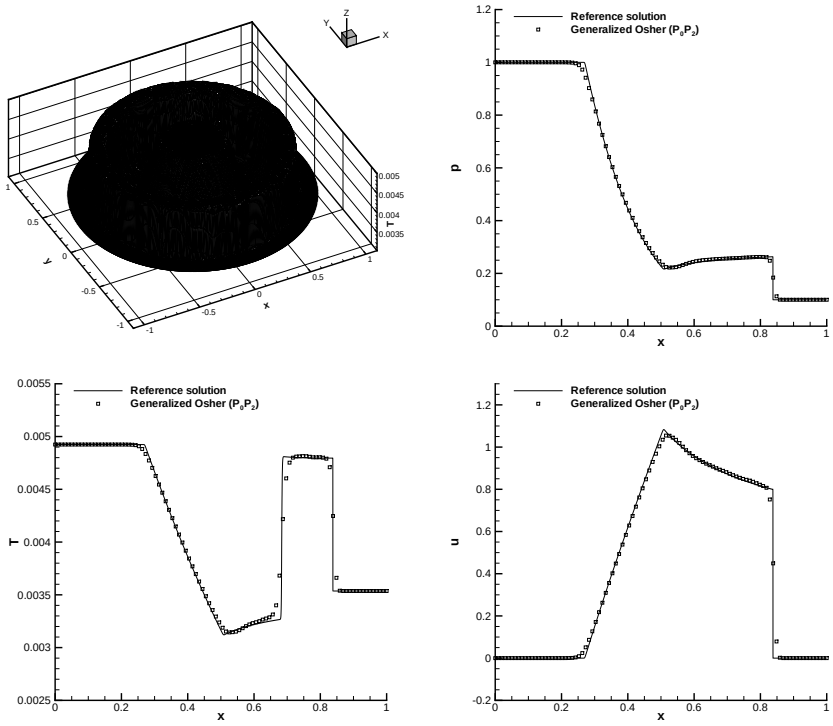

Figure 12: Two-dimensional explosion problem (EP) for the Euler equations with van der Waals EOS.

Section 5, where we have presented numerical convergence studies up to sixth order in space and time. Finally, we presented some test problems for the Euler equations with real gas EOS. To our knowledge, this is the first time that an Osher-type flux has been constructed for such complicated systems as MHD, RMHD, nonlinear elasticity and Euler equations with real gas EOS.

Summarizing, the main advantages of the Osher method over other Riemann solvers are the following: first, it is a *complete* Riemann solver, i.e., it contains all the characteristic fields of the Riemann problem. This is a major advantage over the simpler centered schemes or incomplete Riemann solvers. Then, the Osher method does *not* need an *entropy fix*, in contrast to the Riemann solver of Roe [35] or other linearized Riemann solvers. Moreover, the Osher scheme is *differentiable* with respect to the left and the right state, which makes it particularly well-suited for implicit time-stepping schemes that need the Jacobian of the space discretization operator with respect to the numerical solution.

Further work will be carried out to extend our new approach to more complicated equations of state, that are given, for example, only in tabulated form, or in terms of more complicated analytical expressions, such as for example the Redlich-Kwong-Soave EOS. Future research will also concern the implementation of the new Osher-type flux in implicit time-stepping schemes, where the differentiability of the numerical flux should be of great use when used within a Newton-Krylov technique.

Acknowledgments

The research presented in this article was financed by the Italian Ministry of Research (MIUR) under the project PRIN 2007 and by MIUR and the British Council under the project *British-Italian Partnership Programme for young researchers 2008-2009*. The authors especially would like to thank S.A.E.G. Falle, B. Giacomazzo, O. Zanotti, V. A. Titarev and C. Castro for providing the exact Riemann solvers for the MHD and RMHD equations, as well as for the equations of nonlinear elasticity and the Euler equations with general EOS, respectively. The authors would also like to thank D. S. Balsara for providing the eigenvectors and eigenvalues of the classical and relativistic MHD equations.

A FORTRAN 95 sample code

The simplicity and generality of the new Osher-type scheme presented in this article is best illustrated in the following with a few lines of FORTRAN 95 sample code. All the first order one-dimensional examples presented in this article have all been run with the same computer code, where only the fluxes and eigenvectors of the PDE have been exchanged. For systems where the eigenstructure is not available analytically, it has been computed with the **RG** subroutine of the EISPACK linear algebra package.

A.1 Computation of the Osher-Type dissipation matrix

```
SUBROUTINE OsherMatrix(absA,QL,QR,nVar)
  IMPLICIT NONE
  INTEGER, PARAMETER :: nGP = 3 ! no. of Gauss-Legendre points
  INTEGER  :: i,nVar ! nVar = no. of variables in the PDE
  REAL     :: absA(nVar,nVar),QL(nVar),QR(nVar)
  REAL     :: sGP(nGP), wGP(nGP)
  REAL     :: A(nVar,nVar), Q(nVar)
  REAL     :: R(nVar,nVar), iR(nVar,nVar), L(nVar,nVar)
  INTENT(OUT)   :: absA
  INTENT(IN)    :: QL,QR,nVar
  ! Definition of the Gauss-Legendre quadrature rule
  sGP = (/ 0.5-sqrt(15.)/10., 0.5, 0.5+sqrt(15.)/10. /)
  wGP = (/ 5./18., 8./18., 5./18. /)
  ! Initialize matrix with zero
  absA = 0.
  ! Numerical computation of the path integral along segment path
  DO i = 1, nGP
    Q = QL + sGP(i)*(QR-QL)
    CALL PDEEigenvectors(A,R,L,iR,Q,nVar)
    absA = absA + wGP(i)*MATMUL(R,MATMUL(ABS(L),iR))
  ENDDO
END SUBROUTINE OsherMatrix
```

Here, `PDEEigenvectors` is a subroutine that returns for each state `Q` at the current Gaussian quadrature point `i` the Jacobian matrix `A` of the PDE, the associated right eigenvector matrix `R` and its inverse `iR` as well as the corresponding diagonal eigenvalue matrix `L`. Even if the eigenstructure is not known analytically, it can be computed in a fully numerical way by standard linear algebra software. The subroutine computes the path-integral of the absolute value of $\mathbf{A}$ along the segment path according Eq. (3.5) using the three Gaussian quadrature points given in (4.1). This subroutine is then called from the finite volume scheme sketched in the next subsection. If higher accuracy of the integration is required, one could either resort to even higher order Gaussian quadrature rules [38] or use some adaptive integration strategy, such as for example Romberg integration.

A.2 Sketch of a first order finite volume scheme based on the new general Osher-Type Riemann solver

The following sample code of the main loop of a first order finite volume scheme based on the new general Osher-type Riemann solver makes use of the subroutine `OsherMatrix` presented in the previous subsection. It furthermore uses a subroutine called `PDEFlux` that is supposed to return the physical flux $\mathbf{F}(\mathbf{Q})$.

```
q1 = q
DO n = 1, NMAX
  !  Computation of the physical fluxes for all cells
  DO i = 1, IMAX
    CALL PDEFlux(f(:,i),q(:,i))
  ENDDO
  !  First order FV scheme using the new general Osher-type flux
  DO i = 2, IMAX-1
    CALL OsherMatrix(absA,q(:,i),q(:,i+1),nVar)
    fp = 0.5*(f(:,i+1)+f(:,i))-0.5*MATMUL(absA,q(:,i+1)-q(:,i))
    CALL OsherMatrix(absA,q(:,i-1),q(:,i),nVar )
    fm = 0.5*(f(:,i)+f(:,i-1))-0.5*MATMUL(absA,q(:,i)-q(:,i-1))
    q1(:,i) = q(:,i)-dt/dx*(fp-fm)
  ENDDO
  !  Advance time and write solution back
  time = time + dt
  q = q1
ENDDO
```

Here, `IMAX` is the number of cells in x-direction, `NMAX` is the number of time steps and `dt` and `dx` denote the time step and the mesh spacing, respectively. The variables `f`, `q` and `q1` have dimension `(1:nVar,1:IMAX)`, where `nVar` is the number of variables of the PDE, as in the previous subsection. The boundary conditions in the above code sample are supposed to be Dirichlet boundaries, consistent with the initial condition of the problem, which is appropriate for all shock tube problems presented in this paper.

B Verification of the entropy condition for Burgers equation

In this appendix, we prove that for particular quadrature rules our new generalized Osher-type scheme is entropy satisfying for the nonlinear Burgers equation

$$\frac{\partial u}{\partial t}+\frac{\partial}{\partial x}\Big(\frac{1}{2}u^2\Big)=0, \qquad f(u)=\frac{1}{2}u^2, \qquad A(u)=\frac{\partial f}{\partial u}=u. \tag{B.1}$$

According to [28,30] a monotone, entropy-satisfying numerical flux (*e*-flux) must satisfy the relation

$$E(u_0,u_1)=\int_{u_0}^{u_1}\Big(f(u)-f_{i+\frac{1}{2}}(u_0,u_1)\Big)du\geq 0, \tag{B.2}$$

where $E(u_0,u_1)$ is the entropy production, u_0 and u_1 are the left and right states, respectively, and $f_{i+1/2}$ is the numerical flux function. For fluxes $f_{i+1/2}$ satisfying (B.2), Jiang and Shu were able to prove a cell-entropy-inequality and hence nonlinear stability of DG finite element schemes in L_2-norm, see [28] for details of the proof.

For the case of Burger's equation, our new Osher-type flux (3.5) becomes

$$f_{i+\frac{1}{2}}(u_0,u_1)=\frac{1}{4}(u_0^2+u_1^2)-\frac{1}{2}\sum_j\big(\omega_j|u_0+s_j(u_1-u_0)|\big)(u_1-u_0). \tag{B.3}$$

Inserting the expression of the flux (B.3) into the entropy production function $E(u_0,u_1)$ and application of some basic algebraic manipulations yields the following result:

$$E(u_0,u_1)=\Big(\frac{1}{2}\sum_j\big(\omega_j|u_0+s_j(u_1-u_0)|\big)-\frac{1}{12}(u_1-u_0)\Big)(u_1-u_0)^2:=E_1(u_0,u_1)(u_1-u_0)^2. \tag{B.4}$$

Since the second term is quadratic, it is always greater or equal zero. It is therefore sufficient to show that the first term in brackets, abbreviated by $E_1(u_0,u_1)$, is not negative. In the following, we prove that condition (B.2) is verified for three particular quadrature rules, namely for the trapezoidal rule and Gauss-Legendre quadrature rules using two and three quadrature points. We furthermore show that the entropy condition is **not** satisfied for the midpoint rule, which is the quadrature rule for which the Osher-type scheme (3.5) coincides with the Roe-type scheme (3.6).

B.1 Trapezoidal rule

For the trapezoidal rule we have $s_1=0$, $s_2=1$ and $\omega_1=\omega_2=1/2$. Hence, the crucial term $E_1(u_0,u_1)$ in the entropy production function becomes

$$E_1(u_0,u_1)=\frac{1}{12}\big(3(|u_0|+|u_1|)-(u_1-u_0)\big)\geq 0, \quad \forall u_0,u_1\in\mathbb{R}. \tag{B.5}$$

Clearly, the term $E_1(u_0,u_1)$ is larger than zero for all combinations of left and right states u_0 and u_1.

B.2 Midpoint rule

For the midpoint rule we have $s_1=1/2$ and $\omega_1=1$. In this case the term $E_1(u_0,u_1)$ reduces to

$$E_1(u_0,u_1)=\Big(\frac{1}{4}|(u_0+u_1)|-\frac{1}{12}(u_1-u_0)\Big). \tag{B.6}$$

It is evident that the term E_1 can also become negative, for example whenever $u_1>0$ and $-2u_1<u_0<-u_1/2$.

B.3 Gauss-Legendre rules

Any general Gauss-Legendre quadrature rule must satisfy at least two consistency conditions that correspond to an exact integration of polynomials of up to degree one:

$$\sum_j \omega_j=1 \quad \text{and} \quad \sum_j \omega_j s_j=\frac{1}{2}. \tag{B.7}$$

For the case $u_1\leq u_0$ (shock wave), the term $(u_1-u_0)/12$ in (B.4) is less or equal zero, hence the relevant term E_1 for the entropy production is trivially greater or equal zero. If $u_1>u_0$ and $u_0\geq 0$, $u_1\geq 0$ we obtain

$$E_1(u_0,u_1)=\frac{1}{2}\sum_j\Big(\omega_j(u_0+s_j(u_1-u_0))\Big)-\frac{1}{12}(u_1-u_0), \tag{B.8}$$

and with the consistency conditions of the quadrature rules (B.7) we get

$$E_1(u_0,u_1)=\frac{1}{6}(2u_0+u_1)\geq 0. \tag{B.9}$$

In a similar way one can prove for all $u_1>u_0$ with $u_0<0$, $u_1<0$ that

$$E_1(u_0,u_1)=-\frac{1}{6}(u_0+2u_1)>0. \tag{B.10}$$

What remains at the end is to analyze the important last case $u_1>u_0$ with $u_0<0$ and $u_1>0$, i.e., the *sonic* rarefaction where the Jacobian crosses zero and which is exactly the case where the simple midpoint rule fails. We give results for the case $u_1>u_0$, $u_0<0$ and $u_1>0$ for two particular quadrature rules in what follows:

B.3.1 Two quadrature points

For the particular two-point Gauss-Legendre rule we have $s_{1,2}=1/2\mp\sqrt{3}/6$ and $\omega_1=\omega_2=1/2$. In this case the crucial term $E_1(u_0,u_1)$ in the entropy production function becomes

$$E_1(u_0,u_1)=\frac{1}{2}\Big[\Big(\frac{1}{2}|u_0+s_1(u_1-u_0)|+\frac{1}{2}|u_0+s_2(u_1-u_0)|\Big)-\frac{1}{12}(u_1-u_0)\Big]. \tag{B.11}$$

If the terms under the absolute value operators are both positive or zero, we immediately get the result (B.9) and in a similar way we obtain (B.10) if both terms are negative. The only open case is now if the term under the first absolute value operator is negative and the term under the second one is positive, i.e.,

$$u_0+s_1(u_1-u_0)<0 \quad \text{and} \quad u_0+s_2(u_1-u_0)>0. \tag{B.12}$$

In this case we get after some algebraic manipulations

$$E_1(u_0,u_1)=\frac{\sqrt{3}-1}{12}(u_1-u_0)>0, \tag{B.13}$$

hence for *all* possible cases the entropy production function $E(u_0,u_1)\geq 0$ is greater or equal zero when a two-point Gauss-Legendre quadrature rule is used.

B.3.2 Three quadrature points

For the three-point Gauss-Legendre rule we have $s_{1,3}=1/2\mp\sqrt{15}/10$, $s_2=1/2$, $\omega_1=\omega_3=5/18$ and $\omega_2=8/18$. In this case the term $E_1(u_0,u_1)$ in the entropy production function becomes

$$E_1(u_0,u_1)=\frac{1}{2}\Big(\frac{5}{18}|\psi(s_1)|+\frac{8}{18}|\psi(s_2)|+\frac{5}{18}|\psi(s_3)|-\frac{1}{12}(u_1-u_0)\Big), \tag{B.14}$$

with $\psi(s)=u_0+s(u_1-u_0)$. If the terms $\psi(s_i)$ under the absolute value operators are either all positive or all negative, we obtain immediately the results given in (B.9) and (B.10), respectively. Otherwise, we have the following three cases:

- $\psi(s_1)<0$, $\psi(s_2)>0$, $\psi(s_3)>0$, which requires $u_0>-u_1$ and thus leads for this case to
$$E_1(u_0,u_1)=0.08686u_0+0.13536u_1>0. \tag{B.15}$$
- $\psi(s_1)<0$, $\psi(s_2)=0$, $\psi(s_3)>0$, leading to
$$E_1(u_0,u_1)=0.02425(u_1-u_0)>0. \tag{B.16}$$
- $\psi(s_1)<0$, $\psi(s_2)<0$, $\psi(s_3)>0$, which requires $u_0<-u_1$ and thus leads to
$$E_1(u_0,u_1)=-0.13536u_0-0.08686u_1>0. \tag{B.17}$$

We therefore have shown that also when using the three-point Gauss-Legendre quadrature rule our generalized Osher-type scheme satisfies the entropy condition.

In a very similar manner it is also possible to show that the four-point Gauss-Legendre rule leads to an entropy satisfying Osher-type scheme (3.5). We conjecture that this holds for any Gauss-Legendre rule with more than one point.

References

[1] D. Balsara, Total variation diminishing scheme for relativistic magnetohydrodynamics, Astrophys. J. Supp. Ser., 132 (2001), 83–101.

[2] P. T. Barton, D. Drikakis, E. Romenski and V. A. Titarev, Exact and approximate solutions of riemann problems in non-linear elasticity, J. Comput. Phys., 228 (2009), 7046–7068.

[3] A. Canestrelli, M. Dumbser, A. Siviglia and E. F. Toro, Well-balanced high-order centered schemes on unstructured meshes for shallow water equations with fixed and mobile bed, Adv. Water. Res., 33 (2010), 291–303.

[4] C. E. Castro and E. F. Toro, Solvers for the high-order Riemann problem for hyperbolic balance laws, J. Comput. Phys., 227 (2008), 2481–2513.

[5] M. J. Castro, J. M. Gallardo and C. Parés, High-order finite volume schemes based on reconstruction of states for solving hyperbolic systems with nonconservative products, applications to shallow-water systems, Math. Comput., 75 (2006), 1103–1134.

[6] A. Dedner, F. Kemm, D. Kröner, C.-D. Munz, T. Schnitzer and M. Wesenberg, Hyperbolic divergence cleaning for the MHD equations, J. Comput. Phys., 175 (2002), 645–673.

[7] M. Dumbser, Arbitrary high order PNPM schemes on unstructured meshes for the compressible Navier-Stokes equations, Comput. Fluids., 39 (2010), 60–76.

[8] M. Dumbser and D. S. Balsara, High-order unstructured one-step PNPM schemes for the viscous and resistive MHD equations, CMES-Comput. Model. Eng. Sci., 54 (2009), 301–333.

[9] M. Dumbser, D. S. Balsara, E. F. Toro and C. D. Munz, A unified framework for the construction of one-step finite-volume and discontinuous Galerkin schemes, J. Comput. Phys., 227 (2008), 8209–8253.

[10] M. Dumbser, M. Castro, C. Parés and E. F. Toro, ADER schemes on unstructured meshes for non-conservative hyperbolic systems: applications to geophysical flows, Comput. Fluids., 38 (2009), 1731–2748.

[11] M. Dumbser, C. Enaux and E. F. Toro, Finite volume schemes of very high order of accuracy for stiff hyperbolic balance laws, J. Comput. Phys., 227 (2008), 3971–4001.

[12] M. Dumbser, A. Hidalgo, M. Castro, C. Parés and E. F. Toro, FORCE schemes on unstructured meshes II: non-conservative hyperbolic systems, Comput. Methods. Appl. Mech. Eng., 199 (2010), 625–647.

[13] M. Dumbser and M. Käser, Arbitrary high order non-oscillatory finite volume schemes on unstructured meshes for linear hyperbolic systems, J. Comput. Phys., 221 (2007), 693–723.

[14] M. Dumbser, M. Käser, V. A Titarev and E. F. Toro, Quadrature-free non-oscillatory finite volume schemes on unstructured meshes for nonlinear hyperbolic systems, J. Comput. Phys., 226 (2007), 204–243.

[15] M. Dumbser and C. D. Munz, Building blocks for arbitrary high order discontinuous Galerkin schemes, J. Sci. Comput., 27 (2006), 215–230.

[16] M. Dumbser and O. Zanotti, Very high order PNPM schemes on unstructured meshes for the resistive relativistic MHD equations, J. Comput. Phys., 228 (2009), 6991–7006.

[17] B. Einfeldt, C. D. Munz, P. L. Roe and B. Sjögreen, On Godunov-type methods near low densities. J. Comput. Phys., 92 (1991), 273–295.

[18] S.A.E.G. Falle, On the inadmissibility of non-evolutionary shocks, J. Plasma. Phys., 65 (2001), 29–58.

[19] B. Giacomazzo and L. Rezzolla, The exact solution of the Riemann problem in relativistic magnetohydrodynamics, J. Fluid. Mech., 562 (2006), 223–259.

[20] S. K. Godunov, Finite difference methods for the computation of discontinuous solutions of

the equations of fluid dynamics, Mat. Sb., 47 (1959), 271–306.
[21] S. K. Godunov and E. I. Romenski, Nonstationary equations of the nonlinear theory of elasticity in Euler coordinates, J. Appl. Mech. Tech. Phys., 13 (1972), 868–885.
[22] S. K. Godunov and E. I. Romenski, Thermodynamics, conservation laws, and symmetric forms of differential equations in mechanics of continuous media, in Computational Fluid Dynamics Review, pages 19–31, John Wiley, NY, 1995.
[23] S. K. Godunov and E. I. Romenski, Elements of Continuum Mechanics and Conservation Laws, Kluwer Academic/Plenum Publishers, 2003.
[24] A. Harten, B. Engquist, S. Osher and S. Chakravarthy, Uniformly high order essentially non-oscillatory schemes, III, J. Comput. Phys., 71 (1987), 231–303.
[25] A. Harten, P. D. Lax and B. van Leer, On upstream differencing and Godunov-type schemes for hyperbolic conservation laws, SIAM Rev., 25(1) (1983), 35–61.
[26] V. Honkkila and P. Janhunen, HLLC solver for ideal relativistic MHD, J. Comput. Phys., 223 (2007), 643–656.
[27] C. Hu and C. W. Shu, Weighted essentially non-oscillatory schemes on triangular meshes, J. Comput. Phys., 150 (1999), 97–127.
[28] G. Jiang and C. W. Shu, On a cell entropy inequality for discontinuous Galerkin methods, Math. Comput., 62 (1994), 531–538.
[29] P. D. Lax, Weak solutions of nonlinear hyperbolic equations and their numerical approximation, Commun. Pure. Appl. Math., 7 (1954), 159–193.
[30] S. Osher, Riemann solvers, the entropy condition and difference approximations, SIAM J. Numer. Anal., 21 (1984), 217–235.
[31] S. Osher and F. Solomon, Upwind difference schemes for hyperbolic conservation laws, Math. Comput., 38 (1982), 339–374.
[32] C. Parés, Numerical methods for nonconservative hyperbolic systems: a theoretical framework, SIAM J. Numer. Anal., 44 (2006), 300–321.
[33] J. Qiu, M. Dumbser and C. W. Shu, The discontinuous Galerkin method with Lax-Wendroff type time discretizations, Comput. Methods. Appl. Mech. Eng., 194 (2005), 4528–4543.
[34] L. Rezzolla and O. Zanotti, An improved exact Riemann solver for relativistic hydrodynamics, J. Fluid. Mech., 449 (2001), 395–411.
[35] P. L. Roe, Approximate Riemann solvers, parameter vectors, and difference schemes, J. Comput. Phys., 43 (1981), 357–372.
[36] P. L. Roe and D. S. Balsara, Notes on the eigensystem of magnetohydrodynamics, SIAM J. Appl. Math., 56 (1996), 57–67.
[37] V. V. Rusanov, Calculation of interaction of non-steady shock waves with obstacles, J. Comput. Math. Phys. USSR., 1 (1961), 267–279.
[38] A. H. Stroud, Approximate Calculation of Multiple Integrals, Prentice-Hall Inc., Englewood Cliffs, New Jersey, 1971.
[39] V. A. Titarev, E. I. Romenski and E. F. Toro, MUSTA-type upwind fluxes for non-linear elasticity, Int. J. Numer. Methods. Eng., 73 (2008), 897–926.
[40] V. A. Titarev and E. F. Toro, ADER: Arbitrary high order Godunov approach, J. Sci. Comput., 17 (2002), 609–618.
[41] V. A. Titarev and E. F. Toro, ADER schemes for three-dimensional nonlinear hyperbolic systems, J. Comput. Phys., 204 (2005), 715–736.
[42] E. F. Toro, Shock-Capturing Methods for Free-Surface Shallow Flows, Wiley, 2001.
[43] E. F. Toro, Riemann Solvers and Numerical Methods for Fluid Dynamics, Springer, third edition, 2009.

[44] E. F. Toro and S. J. Billet, Centered TVD schemes for hyperbolic conservation laws, IMA J. Numer. Anal., 20 (2000), 44–79.
[45] E. F. Toro, A. Hidalgo and M. Dumbser, FORCE schemes on unstructured meshes I: conservative hyperbolic systems, J. Comput. Phys., 228 (2009), 3368–3389.
[46] E. F. Toro, M. Spruce and W. Speares, Restoration of the contact surface in the Harten-Lax-van Leer Riemann solver, J. Shock. Waves., 4 (1994), 25–34.
[47] M. Torrilhon, Non-uniform convergence of finite volume schemes for Riemann problems of ideal magnetohydrodynamics, J. Comput. Phys., 192 (2003), 73–94.
[48] I. Toumi, A weak formulation of Roe's approximate Riemann solver, J. Comput. Phys., 102 (1992), 360–373.
[49] J. D. van der Waals, Over de Continuiteit van den Gas-en Vloei Stof Toestand, PhD thesis, University of Leiden, 1873.
[50] B. van Leer, Towards the ultimate conservative difference scheme V: a second order sequel to Godunov's method, J. Comput. Phys., 32 (1979), 101–136.
[51] L. Del Zanna, N. Bucciantini and P. Londrillo, An efficient shock-capturing central-type scheme for multidimensional relativistic flows II: magnetohydrodynamics, Astr. Astrophys., 400 (2003), 397–413.